DOE/MC/30175 -- 5033
(DE96000569)

Portable Sensor for Hazardous Waste

Topical Report
October 1993 - September 1994

Dr. Lawrence G. Piper

October 1994

Work Performed Under Contract No.: DE-AC21-93MC30175

For

U.S. Department of Energy
Office of Environmental Management
Office of Technology Development
Washington, DC

U.S. Department of Energy
Office of Fossil Energy
Morgantown Energy Technology Center
Morgantown, West Virginia

By
Physical Sciences Inc.
Andover, Massachusetts

DISCLAIMER

DOE/MC/30175 -- 5033
(DE96000569)

Portable Sensor for Hazardous Waste

Topical Report
October 1993 - September 1994

Dr. Lawrence G. Piper

Work Performed Under Contract No.: DE-AC21-93MC30175

For

U.S. Department of Energy
Office of Environmental Management
Office of Technology Development
1000 Independence Avenue
Washington, DC 20585

U.S. Department of Energy
Office of Fossil Energy
Morgantown Energy Technology Center
P.O. Box 880
Morgantown, West Virginia 26507-0880

By
Physical Sciences Inc.
20 New England Business Center
Andover, Massachusetts 01810-1022

October 1994

TABLE OF CONTENTS

TABLE OF CONTENTS (Continued)

LIST OF FIGURES

LIST OF FIGURES (Continued)

LIST OF FIGURES (Continued)

LIST OF FIGURES (Continued)

ABSTRACT

We describe an innovative technique to detect hazardous materials at sub part-per-billion levels. Our approach exploits active nitrogen energy-transfer (ANET) to excite atomic and molecular fluorescence characteristic of various hazardous species. ANET excitation is very state specific, generating simple spectra that are easily detected with instrumentation of modest resolution. Typical spectral features include 254 nm emission from Hg, 388 and 420 nm emission from CN when organics are sampled, and 278 nm emission from CCl when chlorinated organics are sampled. We also observe several broadbands between 450 and 540 nm where uranium compounds are added to the D-B discharge region. We attribute this spectrum to electronic transitions of uranium oxide, probably UO. Additionally, we have used ANET to detect a number of heavy metals such as Cr, Se, Cd, Pb, and Cu.

Dielectric-barrier (D-B) discharge technology generates the active nitrogen. This approach affords atmospheric-pressure operation, fluorescence excitation in gaseous, particulate, and aqueous sample matrices, and is amenable to field operation because the discharge and associated electronics are compact and can be powered by 12V batteries.

This report details the results of the first phase of a three and a half year program designed to develop a portable monitor for sensitive hazardous waste detection. The ultimate goal of the program is to develop our concept to the prototype instrument level. In this first phase we have demonstrated the applicability of the ANET technology to a variety of hazardous species, and have determined detection sensitivity limits for Hg, Se, organics, and chlorinated organics to be at part-per-billion levels or below.

EXECUTIVE SUMMARY

This report details the results of the first phase of a three and a half year program designed to develop a portable monitor for sensitive hazardous waste detection. The ultimate goal of the program is to develop our concept to the prototype instrument level. Our prototype will be a compact, portable instrument that will allow real-time, *in situ* monitoring of hazardous wastes. Our instrument will be able to provide rapid field screening of hazardous waste sites to map out the areas of greatest contamination. Remediation efforts will then be able to focus on these sites. Further, our instrument will be able to indicate whether or not clean-up technologies are successful at reducing hazardous materials concentrations below regulated levels, and will provide feedback to allow changes in remediation operations, if necessary, to enhance their efficacy.

The primary goals of this first phase of the program were two fold:

- to demonstrate the variety of hazardous species that can be detected by the technique of active nitrogen energy transfer (ANET) excitation of atomic and molecular fluorescence, for hazardous species of interest to DOE; possible species of interest might include heavy metals, organics and chlorinated organics, and/or transuranic surrogates; and

- to demonstrate sensitivity limits for detecting several of these species at parts per billion (ppb) levels.

The criteria for success in the first phase of this program were that we achieve the two goals listed above. As we demonstrate in the body of this report, we have met these success criteria and are now prepared to begin the Phase II work. In Phase II we will develop a breadboard device and design the prototype instrument that will be constructed and tested in Phase III. The Phase I results clearly demonstrate the extreme sensitivity offered by the D-B ANET approach. In addition, the unit can be powered by a simple 12 volt battery, and this means that a compact, portable, and field worthy sensor can be developed.

To achieve these goals, we designed a program whereby we would first focus on the ANET technique and study parameters important for the production and quenching of the nitrogen metastables that are the primary component of the active nitrogen produced in our atmospheric pressure dielectric-barrier discharge. The second component of the program was qualitative and quantitative studies on the detection of a number of hazardous species including heavy metals, both chlorinated- and non-chlorinated-organic molecules, and the transuranic surrogates, U and Th. The third component of the program was to investigate the effects of adding small quantities of dust to the D-B discharge region. The two issues to resolve in this part of the investigation were whether the presence of dust compromised the operation of the D-B discharge and whether species adhering to the dust could be detected.

Our technique, discussed in more detail below, is to excite atomic and molecular fluorescence by the technique of active nitrogen energy transfer (ANET). The active nitrogen is made in

a dielectric-barrier (D-B) discharge operating in nitrogen at atmospheric pressure. Only a limited number of emission lines or bands are excited for each hazardous species, so spectral resolution requirements are greatly simplified over those of other spectroscopic techniques. The dielectric-barrier discharge is compact, 1 to 2 cm in diameter and 1 to 10 cm long. Furthermore, the discharge power requirements are quite modest, so that the unit can be powered by batteries. Thus the an instrument based on ANET can readily be made portable.

We summarize our results here. The body of the report details them.

We used optical tracer diagnostics to investigate nitrogen metastable production and quenching in the D-B discharge. We found that metastable production was optimum when the discharge was operated at atmospheric pressure and at higher discharge voltages. Our D-B lamps were all of annular geometry. Metastable production didn't appear to be a strong function of the annular gap spacing. In addition, metastable production was satisfactory for lamps made from Pyrex®, fused quartz, and alumina. Nitrogen metastable quenching by O_2 was relatively efficient, that by CO_2 and H_2O much less so. In the absence of added gas, metastable quenching was dominated by molecular nitrogen or the part-per-million levels of impurities in the nitrogen used in the D-B lamp.

In this program we demonstrated the detection of the heavy metals Hg, Cr, and Se. We showed that ANET generated a simple spectrum from all three metals that could be easily distinguished from background emissions in the D-B lamp. Our measurements showed a linear variation in intensity of ANET excited emissions as a function of the number density of these metals added to the discharge region. The ultimate detection sensitivity for Hg and Se detection is well below part-per-billion (ppb) levels, while that for Cr appeared to be just below part-per-million (ppm) levels. We think our number density measurements for the Cr compound must be in error and that sensitivity for it is also at sub ppb levels.

All organic species studied evinced strong emission from CN radicals at 388 and 420 nm. All chlorinated organic species investigated showed CCl emission at 278 nm. In a few instances we also observed weak emission from CH radicals at 431 nm from the addition of organic molecules. A few attempts to detect oxygenated organics by observing emission from OH radicals at 283 or 308 nm were unsuccessful. Detection limits for the organic species were about 5 ppb at both 388 and 278 nm.

Our investigations on the effects of particulates on the operation of the D-B discharge involved first observing that particles in the discharge region didn't appear to affect strongly the ANET process. That is, heavy metal and organic species were still readily detectable when particles were present in the discharge region. Second, we made a simulated cement with a mean particle size distribution below 10 μm and spiked it with a few drops of a mercuric nitrate solution. We then observed that upon introducing these particles to the D-B discharge region, the mercury on the particles was manifested by the appearance of the 254 nm mercury line. Finally, we observed that adding powered uranyl (UO_2^*) compounds to the D-B discharge region resulted in molecular emissions, probably from UO, between 480 and 540 nm.

In addition to the detailed description of our Phase I effort, this report also outlines our plans for Phase II. In Phase II we will design, construct, and test a breadboard ANET sensor in Task 2.1. Using the results of Task 2.1, we will then complete a design of the portable monitor that will be built in Phase III.

1. INTRODUCTION

Hazardous materials, especially heavy metals and certain organic molecules, particularly chlorinated ones, have become a ubiquitous environmental problem. Our country is spotted with a number of sites in which hazardous waste has been deposited. In some instances hazardous materials were unthinkingly dumped in ponds and land fills. In other instances the materials were sealed in containers before being buried or land filled. In many instances, these containers have begun leaking and releasing their waste to the environment. Another on-going source of hazardous waste is the emissions from various combustion activities such as coal-fired power plants, incinerators for municipal and hazardous wastes, and crematoria. A third site of hazardous waste is in buildings and on properties where these various hazardous materials have been used in various activities. For example, mercury was once an important component in a lithium isotope separation process that was used at radioactive materials processing centers. Oak Ridge National Laboratory, for example has nearly nine metric tons of mercury on site. Some of this is safely stored, some remains spread throughout the buildings in which is was used, and some has found its way into local waterways. Other nuclear material processing sites have similar problems.

In many instances the actual locations and distribution of the hazardous materials are well known, but in others all that is known for sure is that hazardous materials are buried out somewhere in a site that may extend over hundreds of acres. Mapping these sites then becomes a problem. Once the identity and exact location of hazardous materials are known, appropriate remediation efforts can begin. It then becomes important to be able to easily quantify the success of these operations so that one can know if more work is needed or if efforts have been effective in reducing hazardous species to levels currently considered safe.

Current analytical technology generally requires samples to be taken from a site in suitable containers and taken to analytical laboratories where they are processed. This approach is expensive and time consuming. Often several weeks will pass before analytical results are reported back to the waste site. Clearly what is needed is a portable, field-operable instrument that can detect various hazardous species in real time. Instrumentation that is sufficiently compact to be transported to and operated in the field tends to lack adequate sensitivity to detect many hazardous species at the low levels required to achieve environmental compliance.

The most common analytical techniques that have been applied to heavy metal contaminant analysis are atomic absorption spectrometry (AAS) and atomic (or optical) emission spectrometry (AES or OES). Samples are usually atomized and excited, where necessary, in a flame or plasma, generally a direct current plasma (DCP) or an inductively coupled plasma (ICP). Although these techniques can detect some species at or below part per billion(ppb) levels[1], for a number of other species, including As, Se, Hg, Pb, Sn, and U, ICP-OES cannot detect samples below 10 ppb. Flame-AA is even worse with limits for these particular species above 100 ppb, except for Pb for which the sensitivity limit is 10 ppb. Some more complex variants of AA (e.g., graphite furnace APC or GFAA) have been used to detect some of these species at sub-ppb levels, but these variants require special sample handling and preparation. In additional to marginal sensitivity limits, some other drawbacks of these common techniques are the following:

- they are not readily adaptable to real-time monitoring. Samples must be extracted and shipped to another lab for analysis;
- they require extensive operator training;
- they are not readily field operable or portable although systems can be placed in a truck for on-site operation; and
- they tend to be expensive to purchase, operate, and maintain.

As we describe below, our approach obviates these problems and offers several distinct advantages including higher sensitivity, field operability, and lower cost.

The detection of organic species is usually effected with some form of chromatography, generally high pressure liquid chromatography (HPLC) or gas chromatography (GC) with either flame ionization detection, or eluent detection by means of mass spectrometry (GC-MS). These systems have many of the drawbacks listed above for the heavy metals. The one advantage they do have over our active nitrogen energy transfer (ANET) technique is that they can identify and quantify individual organic compounds. To date, we have only been able to use ANET to detect total organic content and chlorinated organic content in a sample. We have some strategies to allow us to distinguish aromatic compounds using ANET, but have not as yet tested these in our system. Jurgensen and Winefordner have shown this ability in their D-B discharge system, but their system operated at low pressures. The ability to distinguish aromatic species from other organic compounds at atmospheric pressure remains to be determined.

This section follows with a statement of the overall project objective, followed by a detailed description of the physics and chemistry of the ANET process. Then we discuss our experimental program in detail in Section 4. This includes a discussion of experimental apparatus and techniques, results of experiments aimed at understanding metastable creation and destruction processes in a D-B discharge, and finally, in Subsections 4.3 through 4.6, the results of our measurements on heavy-metal and organic detection, and of detection of Hg and U compounds on particulates.

2. PROJECT OBJECTIVE

The overall objective for this 3-1/2 year program is to develop a portable monitor for hazardous waste that can be used in field tests on building materials. The program is planned in three phases with decision points at the end of each phase to decide whether or not the subsequent phase should be pursued. The initial phase of the program is to demonstrate the applicability of active nitrogen energy transfer (ANET) excitation of fluorescence from hazardous species, using dielectric-barrier (D-B) discharge technology to generate the active nitrogen at atmospheric pressure. The subsequent two phases of the program are to develop the technology to the process level and undertake an engineering design of a portable hazardous waste monitor, and finally, to develop and field test a prototype instrument.

3. THE NATURE OF ANET

Our ANET technique has a number of features that make it an attractive candidate upon which to base an instrument for monitoring hazardous species in a variety of matrices:

- real-time analysis
- multispecies
- sub-part-per-billion sensitivity
- tolerant to dust particles and moisture
- atmospheric pressure operation
- compact (<1 ft^3 excluding gas supply) and light weight (20 to 30 lb)
- low power (<10W discharge power).

Figure 1 shows our approach schematically. Basically, samples introduced into active nitrogen are excited by electronic energy transfer from metastable nitrogen molecules. The electronically excited atoms or molecules then fluoresce and are detected. Because active nitrogen transfer excites only a few levels of the receptor species (see Figure 2), the resultant fluorescence spectrum is relatively simple and can be resolved either by an interference-filter or a small polychromator. In the case of mercury detection, only the line at 253.7 nm is excited with any efficiency. For selenium, two lines at 207.5 and 216.5 nm are excited more than an order of magnitude more efficiently than the lines at 196.0, 204.0, and 206.5 that are prominent in arc spectra. The predominant emissions from organic species are the CN bands at 388 and 415 nm, while chlorination of the organic is signaled by a single band at 278 nm.

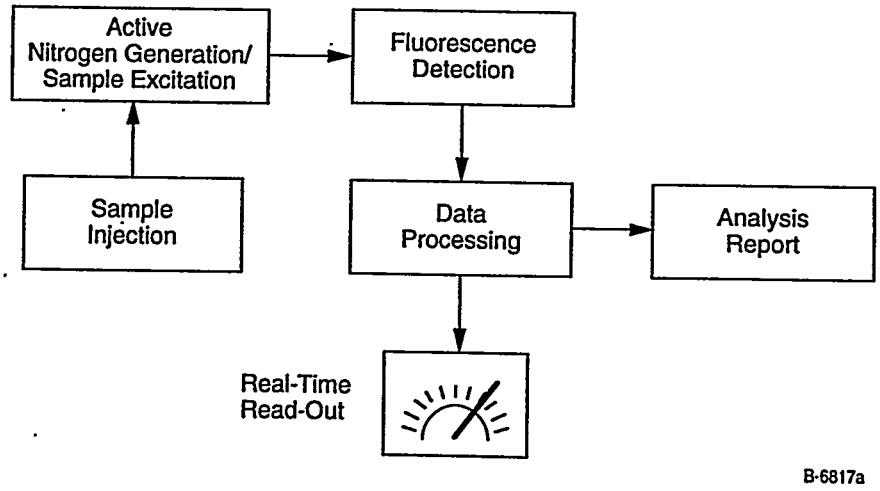

Figure 1. Block diagram of ANET analysis system.

We use a dielectric-barrier discharge in nitrogen at atmospheric pressure to generate the active nitrogen. This approach has several advantages. First, because the system operates at atmospheric pressure, no pumps are needed for the system to work. Second, the nature of the

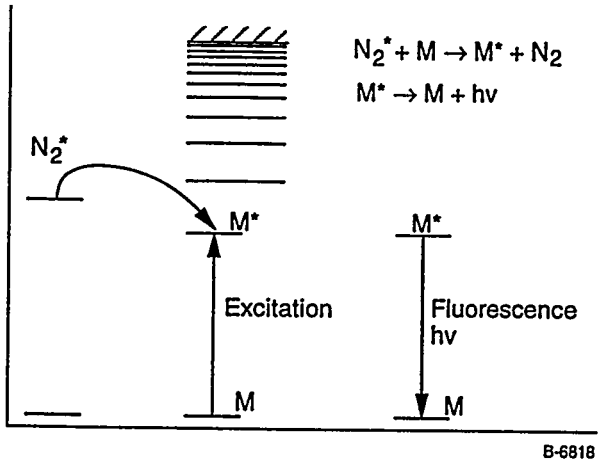

Figure 2. ANET excitation mechanism.

dielectric-barrier discharge is such that small particles below about 2 μm will be vaporized and any contaminants on them can then be detected. Third, commonly used dielectric materials, such as glass or ceramics, provide a discharge-region environment that is inherently clean. Thus, sample contamination by the instrument will not be an issue. Finally, the D-B discharge requires little power to operate efficiently. This means an instrument can be designed to run on batteries, thereby making it suitable for field use.

3.1 Background on ANET

From the beginning of this century, scientists have observed characteristic emissions from atoms and free radicals when atomic and molecular species were added to active nitrogen. A rich literature exists detailing the chemical reactions and energy-transfer processes that occur to excite these emissions.[2-7] Basically, metastable nitrogen molecules in the active nitrogen transfer their energy to the various acceptor species. Most metastable nitrogen energy transfer processes are quite efficient, generally occurring at rates on the order of one-tenth gas kinetic or greater.[8]

Most active nitrogen studies have relied upon the recombination of nitrogen atoms at relatively low pressures to generate the metastable nitrogen molecules. This approach has the disadvantage that considerable power is required to dissociate atomic nitrogen. In addition, because these systems operate at pressures on the order of 1 to 10 Torr, a vacuum system is required. We used such a system to demonstrate the sensitive detection of a number of heavy metals that arise in lubricating oils as a result of engine wear.[9] We observed emission from atomic species such as Pb, Cd, Ni, Cu, Al, and Ag with sensitivities on the order of picograms per gram of sample.

In this program, we demonstrate a novel alternative approach to generating molecular nitrogen metastables that circumvents most of the problems inherent in the atom-recombination-systems. Our approach is to generate the metastables in a dielectric-barrier discharge operating at atmospheric pressure and total powers less than 2W. Thus, our system requires neither a large power source nor a vacuum system. In addition, the overall metastable number densities generated in the dielectric-barrier discharge are several orders of magnitude larger than those in the atom-recombination system. This greatly enhances the sensitivity of our monitor.

3.2 Dielectric-Barrier Discharge Technology

A dielectric-barrier discharge is a high voltage ac discharge between two electrodes, at least one of which is separated from the discharge region by a dielectric barrier (insulator) such as

glass (see Figure 3).[10-13] A typical discharge will run at voltages between 3 and 30 kV at frequencies from line frequency to 100 kHz. Gas pressures are typically an atmosphere and gap spacings are on the order of a few millimeters. In its simplest form, the discharge can be powered by attaching the electrodes to the output of a high voltage, step-up transformer, such as a neon-sign transformer, plugged into a variac.

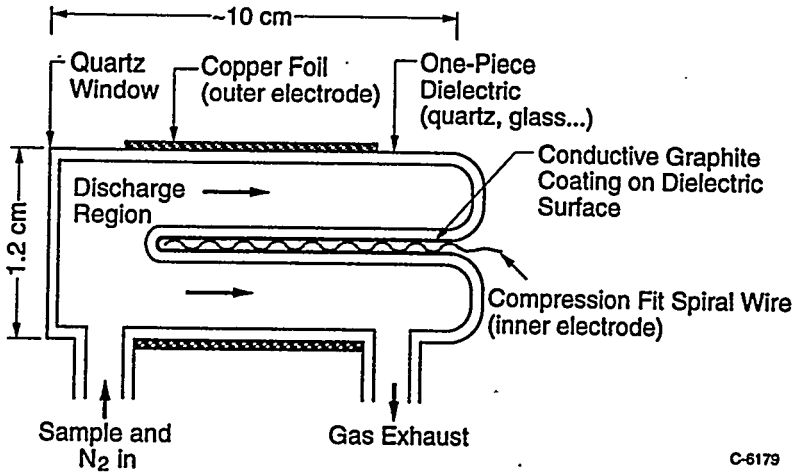

Figure 3. Schematic diagram of D-B discharge lamp.

The dielectric-barrier discharge is often referred to as an ozonizer discharge because it is the discharge used in efficient commercial ozone generators. Thus, such discharges can readily be made rugged and robust. It is not a single discharge in the sense of a continuous arc or glow discharge, but rather a collection of innumerable microdischarges between the dielectric and the other electrode. These microdischarges consist of short duration (typically 10 to 100 ns) current pulses (100 to 1000 A cm^{-2}) localized in roughly cylindrical filaments, typically 100 μm in radius. Although the current *densities* in the microdischarges are quite large, the overall power consumption of a typical dielectric-barrier discharge is relatively modest. Often the total current drain will be only a few milliamps, resulting in an overall power consumption on the order of 10W.

The mean electron energy in the microdischarge is on the order of 1 to 10 eV and can be readily varied by changing the gas pressure and interelectrode gap spacing. Thus one can tune the electron energy of the discharge to selectively enhance the excitation of one species over another. At any given instant in time, the microdischarges are distributed uniformly across the face of the dielectric. This uniformity provides a relatively stable excitation throughout the discharge volume.

Dielectric-barrier discharges in pure nitrogen have been shown to be efficient sources of metastable $N_2(A^3\Sigma_u^+)$, even at pressures of one atmosphere,[14-17] thus providing the active nitrogen source necessary to the selective analyte excitation of ANET. Being able to operate at atmospheric pressure also eliminates any requirements for sophisticated vacuum equipment. In

addition to reducing power and weight requirements, atmospheric pressure operation will greatly simplify sample handling and introduction into an instrument based upon ANET.

The energy in a typical microdischarge, 10 kV, 300 A cm^{-2}, 10 ns duration, and 100 μm radius, is about 10 μJ. This is more than enough energy to vaporize small particles in the discharge region if a microdischarge terminates on them. The minimum energy required to vaporize a dust particle will be equal to the heat necessary to raise the particle temperature to its vaporization point plus the particle's latent heat of vaporization. For a particle of SiO_2, the total energy required to achieve complete vaporization will be about 600 kJ $mole^{-1}$. Thus for a typical particle of size 1 μm radius and density of about 2.5 g cm^{-3}, we calculate that the energy required for complete vaporization is about 0.2 μJ, much less than the energy of a single microdischarge. The resultant vapor then interacts with the active nitrogen and is induced to fluoresce.

3.3 The Chemistry and Physics of ANET

Our analytical technique uses the metastable nitrogen species generated by electron impact in the microdischarges as the fluorescence excitation source. If the analyte species is an atom such as free mercury, the excitation will occur directly. When molecular species are added to the discharge region, the $N_2(A)$ generally reacts with the molecule and produces some characteristic molecular fragments. The $N_2(A)$ subsequently excites these fragment species. For example, when $HgCl_2$ is added to the discharge region, HgCl emission is readily observed around 540 nm. Adding organic molecules results in CN emission at 388 and 420 nm.

The chemical processes responsible for exciting fluorescence from species M in a dielectric-barrier discharge are summarized by the following reactions:

$$N_2 + e^- \rightarrow N_2^* + e^- \quad (1)$$

$$N_2^* + N_2 \rightarrow N_2 + N_2 \quad (2)$$

$$N_2^* + M \rightarrow M^* + N_2(X) \quad (3)$$

$$M^* \rightarrow M + h\nu \quad (4)$$

$$M^* + N_2 \rightarrow M + N_2 \quad (5)$$

$$M^* + Q \rightarrow M + Q' \quad (6)$$

$$N_2^* + Q \rightarrow N_2 + Q' \quad (7)$$

where Q represents a species in the discharge that quenches electronic energy in either the N_2^* or the electronically excited analyte (M^*).

Metastable-nitrogen or analyte-fluorescence quenching can limit the sensitivity of our technique. We found empirically (see Subsection 4.2.3) that O_2 has the major impact upon

sensitivity. The presence of other species, including N_2, CO_2, and H_2O in the discharge have a much smaller impact on metastable number densities or fluorescence intensities. Thus, it is important to limit the amount of O_2 admitted to the discharge. As we show below, O_2 quenching is tolerable and our sensitivity is still excellent even in its presence.

Although the dielectric-barrier discharge is a pulsed discharge, one can analyze it mathematically as if it were a continuous discharge if observations are averaged over a number of discharge cycles. Then, the excited species in the discharge region can be considered to be effectively in steady state and we can write steady state equations describing the intensity of the analyte fluorescence:

$$I_{M^*} = k_4[M^*] = k_3[M][N_2^*]/(1+(k_5/k_4)[N_2] + (k_6/k_4)[Q]) \quad . \tag{8}$$

Equation (8) shows that for constant metastable number density, $[N_2^*]$, and total pressure, the fluorescence intensity will be linearly proportional to the additive number density, [M], provided the number densities of any potential quenchers remain constant. If one maintains a constant sample size, this generally will be the case. The linearity of fluorescence intensity with analyte number density has been demonstrated experimentally to cover four to five orders of magnitude for a number of species.[3-7,14,15] In some instances, the total useful range of number densities spanned by this technique can cover up to seven orders of magnitude in analyte number density. Thus, the applicability of the ANET technique covers a tremendous dynamic range.

The exciting species in active nitrogen generally is considered to be $N_2(A^3\Sigma_u^+)$, although other nitrogen metastables have been invoked from time to time.[2] $N_2(A)$ carries about 6 eV of internal energy. The steady state number density of $N_2(A)$ is given by

$$[N_2^*] = k_1[e^-][N_2]/(k_2[N_2] + k_3[M] + k_7[Q]) \quad . \tag{9}$$

The radiative lifetime[18] of $N_2(A)$ is about 2.5 s. Thus, the primary mechanism for $N_2(A)$ deactivation will be quenching rather than radiative decay.

Even though $N_2(A)$ quenching by most analytes is a relatively efficient process,[8] $k_3 \approx 10^{-12}$ to 10^{-10} cm^3 molecule^{-1} s^{-1}, the analyte's effect on metastable number densities in the D-B discharge will be entirely negligible because its number density is so small. Therefore, the metastable number density will be controlled by the rate of quenching by N_2, a relatively inefficient process ($k_2 \sim 3.5 \times 10^{-16}$ cm^3 molecule^{-1} s^{-1})[19], and by any efficient quenchers admitted with the sample, e.g. O_2 ($k_7(O_2) \sim 3 \times 10^{-12}$ cm^3 molecule^{-1} s^{-1})[20] if the sample is in air. Thus the quantity of admitted sample must be controlled, and the number density of metastables in the discharge region must be monitored so that metastable quenching effects can be included in the data analysis. We will discuss this issue in considerable detail below (Subsection 4.2.3).

Although the nitrogen metastable number density can be monitored (vide infra), and signals thereby normalized to account for any number density changes, one will still need to limit

the size of the sample extracted so as to maintain quenching at manageable levels. This is not a particularly serious restriction, however. If the admitted sample is at the level of 0.1% of the nitrogen in the lamp, and the analyte of interest comprises 1 part per billion of the sample, the analyte number density in the discharge region will still be 10^7 atoms cm^{-3}. In our previous studies for the Navy[9], using the much less efficient N-atom recombination source of active nitrogen, our sensitivity exceeded this level by several orders of magnitude for most species studied. Because mercury is one of the species most easily detected by ANET, we expect sensitivities several orders of magnitude below this. Our experimental results are in accord with this.

In summary, the above discussion shows that ANET has the following advantages as an analytical technique:

- Signals that are linear in concentration of the analyte
- Sensitivities that are at the sub-ppb level
- Required instrumentation is compact with small power requirements
- Most heavy metals have been detected in fluorescence following $N_2(A)$ energy transfer.

4. EXPERIMENTAL ACTIVITIES

Our experimental program had several components. First, we investigated the operation of the dielectric-barrier discharge in pure nitrogen. These studies included characterization of background spectra in the discharge and how the various spectral features varied in intensity as the discharge voltage and pressure were varied. In addition we investigated the variations in intensity of some of these features as a function of number density of certain added species such as O_2, CO_2, and H_2O. The purpose of these studies was to learn about possible metastable quenching processes that might compromise the sensitivity of our technique.

Our central focus, however, was determining the sensitivity of our technique for detecting a number of hazardous materials. We first surveyed the spectral signatures characteristic of a number of hazardous species. Then we determined variations in signal levels as a function of analyte number densities added to the discharge region. In the case of mercury, we detected the effects on the mercury emission levels, at constant Hg number density, when a quenching gas was added to the discharge region. Finally we investigated the ability of our technique to work in the presence of particulates and demonstrated the detection of mercury and uranium compounds adhering to fine particles.

We begin by describing our experimental system, and then detail our measurements and data analysis.

4.1 Experimental Apparatus

Our laboratory experiments used the apparatus shown schematically in Figure 4. It consists of a dielectric-barrier discharge lamp, similar to that illustrated in Figure 3, a power source, an optical multichannel analyzer, and gas handling lines.

We have constructed lamps in both planar and annular geometries[21] using a variety of dielectrics, including Pyrex®, quartz, alumina, and sapphire. Most of our experiments used models similar to that shown schematically in Figure 3 above. They are fabricated from a single piece of quartz having a 12-mm OD body with an axial protrusion inside the 12-mm tube. We used several lamps with various protrusion diameters ranging from 3 to 8 mm OD. The end opposite the protrusion is sealed with a quartz window. Gas enters the lamp through a side arm situated at the end of the lamp nearest the window and exits through another side arm at the opposite end of the lamp body. The general flow of gas away from the window helps maintain a cleaner environment in the discharge region and keeps the window free from the build up of contamination.

The lamp has an annular discharge region. The outer electrode is formed by wrapping copper-foil tape around the outside of the lamp body. The inner electrode is formed by painting the inside of the axial protrusion with a layer of conductive material such as graphite, nickel, or silver. A wire wrapped loosely with copper turnings is inserted into the protrusion and is connected to the power supply. This configuration provides a clean discharge region because all surfaces are quartz.

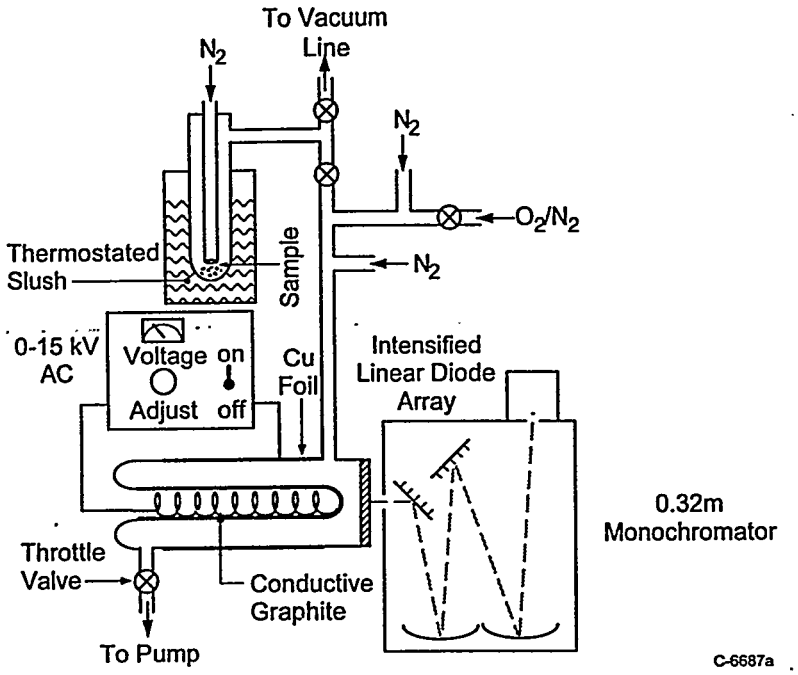

Figure 4. Schematic of laboratory apparatus.

Only one of the two electrodes must be covered by a dielectric. We have made a number of lamps in which the center electrode was a metal rod situated along the lamp body's axis. Such a configuration does not appear to offer any significant advantages in terms of metastable production and does have the potential to contaminate the discharge region. Thus we favor the double dielectric-barrier design.

We have used two different power sources for our dielectric-barrier discharge lamps. For most experiments, we connected the electrodes to the center-tap-grounded secondary of a 15 kV neon sign transformer. The voltage to the primary was controlled by a variac operating off standard 60 Hz ac power. In a few experiments, we connected the electrodes to the secondary of an automotive ignition coil and powered the coil with 12 to 15V square-wave pulses at frequencies between 45 Hz and 3 kHz. This power source is much more compact and light and lends itself to battery operation.[21] Both sources gave similar results.

Volatile samples were placed in a cold finger immersed in a bath that was thermostated for vapor pressure control. A small flow of nitrogen through the cold finger transported volatile samples into the discharge region. The concentration of the analyte in the discharge region was equal the product of the compound's vapor pressure in the cold finger and the dilution factor between the N_2 flow through the cold finger and that through the D-B lamp as a whole. Because most species are so readily detected by ANET, the temperature of the thermostated bath was kept quite cold. Generally, we used slush baths of either $CHCl_3$ (-63°C), methanol (-98°C), or ethanol (-110°C). At these temperatures the vapor pressures of analyte species were between 10^{-5} and 10^{-8} Torr. Intermediate temperatures were achieved by making slush baths from mixtures of water and methanol. The bath temperatures were measured with a thermocouple.

We found it was important to use teflon fittings and tubing in the gas-handling lines exposed to mercury and organic compounds. These species have a tendency to permeate most materials including polyethylene, polypropylene, and stainless steel. If such materials are used, they will soak up analyte. When analyte levels in the sample stream are relatively high, these materials will remove some of them from the sample stream and readings become erroneously low. On the other hand, if analyte levels are relatively low in the sample stream, or even completely absent, these materials will give off analyte and give signals that are erroneously large. In addition, we found that we could maintain a cleaner discharge region when we switched from a Pyrex lamp to one made from fused quartz.

We used an optical multichannel analyzer (OMA) to detect the fluorescence excited in these experiments. This allowed us to survey a variety of wavelengths rapidly so that we could investigate background emissions and how they changed with changes in operating conditions. This was important because the background emissions provide good diagnostics of the conditions in the discharge region. The discharge lamp was placed about 1.5 cm in front of the entrance slit of a 0.32m monochromator. We generally used a 2400 groove mm^{-1} grating, although a few experiments used gratings with 300 or 1200 grooves mm^{-1}. Dispersed emission spectra were recorded by a Princeton Instruments ST210 Optical Multichannel Analyzer (OMA) system with an intensified diode linear array. The lamp was sufficiently bright, that relatively high resolution spectra ($\Delta\lambda$~0.1 nm) could be accumulated with good signal to noise in only 10 s. In some instances, longer accumulation times were used but never in excess of 5 min. Data were stored in a computer for later analysis.

4.2 Dielectric-Barrier Discharge Operational Characteristics

4.2.1 General Observations

Our initial investigations on the operational parameters of our dielectric-barrier (D-B) discharge lamps involved first seeing how some of the background spectral features, i.e., features appearing with only nitrogen in the lamp, scaled with changes in total pressure and voltage. The primary background spectral features are the NO gamma bands, $NO(A^2\Sigma^+ - X^2\Pi)$, nitrogen second-positive bands (2^+), $N_2(C^3\Pi_u - B^3\Pi_g)$, and nitrogen Herman infrared (HIR) bands, $N_2(C''^5\Pi_u - A'^5\Sigma_g^+)$. The gamma bands are excited by energy transfer from metastable nitrogen molecules to NO,[21] the NO being formed in the discharge in reactions involving trace O_2 impurities.

Minor spectral features include the nitrogen first-positive bands (1^+), $N_2(B^3\Pi_g - A^3\Sigma_u^+)$, nitrogen Gaydon-Herman bands, $N_2(H^3\Phi_u - G^3\Delta_g)$, nitrogen first-negative bands (1^-), $N_2^+(B^2\Sigma_u^+ - X^2\Sigma_g^+)$, and $O(^1S - ^1D)$. Among these systems, only the N_2 1^+ bands are excited with any significant efficiency in the atmospheric-pressure D-B lamp, but their appearance is very weak. The bands are quenched very strongly by atmospheric-pressure N_2.[22] Our investigations focussed on just the three strongest band systems.

Figure 5 shows how the intensities of the 2^+, HIR, and gamma bands vary as a function of total pressure in the lamp for a fixed discharge voltage of 7.4 kV. As pressure in the lamp

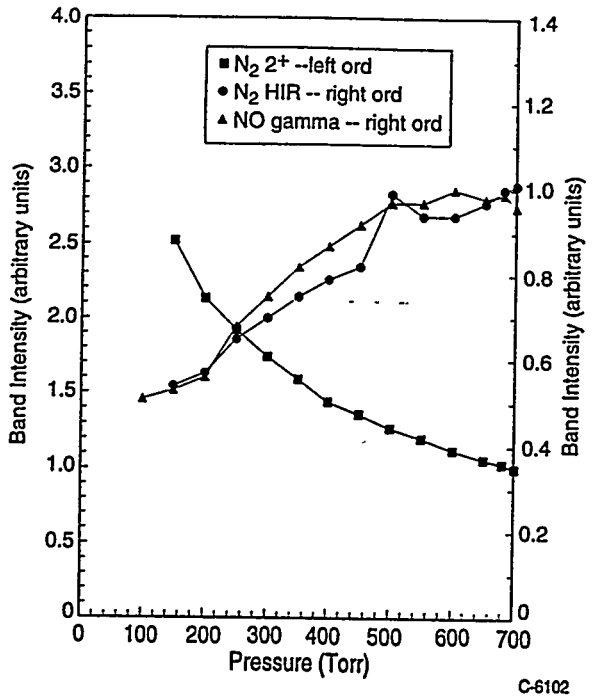

Figure 5. Variation in the relative intensities of the NO gamma bands, $NO(A^2\Sigma^+ - X^2\Pi)$, the nitrogen second-positive bands (2^+), $N_2(C^3\Pi_u - B^3\Pi_g)$, and the nitrogen Herman infrared (HIR) bands, $N_2(C''^5\Pi_u - A'^5\Sigma_u^+)$, as a function of pressure in an N_2 D-B discharge operating at 7.4 kV.

increases, the HIR and gamma bands increase in intensity, whereas the 2^+ intensity drops quite markedly. Exciting the 2^+ bands by electron impact requires electron energies in excess of 11 eV. We attribute the decline in intensity of the 2^+ bands with increasing pressure, therefore, to be an indication that as the pressure increases, the mean electron energy distribution decreases. This is in accord with expectations based upon previous reports.

While almost 11 eV also is required to excite the HIR bands, a different mechanism is responsible for their surprisingly strong excitation in the atmospheric-pressure D-B lamp. We have shown previously that HIR emission can be excited in a reaction where two molecules of $N_2(A^3\Sigma_u^+)$, each containing 6 eV, pool their energies to generate one N_2 molecule in the $C''\ ^5\Pi_u$ state, and one in the ground electronic state.[23] In such an energy-pooling reaction, therefore, the HIR emission intensity is proportional to the square of the nitrogen metastable $N_2(A)$ number density. Thus, variations in the HIR intensity will mirror variations in $N_2(A)$ number density, and we can use HIR emissions as a monitor for $N_2(A)$ concentrations.

Our observations, then, imply that the $N_2(A)$ number density increases with increasing pressure. We expect this to happen for several reasons. First, at the higher pressures, the mean electron energy in the discharge is less, thus favoring excitation of lower energy states. Second, $N_2(A)$ is excited not only by electron impact, but also by quenching of higher energy nitrogen electronic states, principally $N_2(B^3\Pi_g)$. Thus, increasing the lamp pressure will enhance the rate of conversion of these other electronic states to $N_2(A)$. Recall that $N_2(A)$ is the species that excites the analyte fluorescence.

That $N_2(A)$ increases as pressure in the lamp increases is also indicated by the behavior of the NO gamma bands. We have shown that these bands are excited quite efficiently by $N_2(A)$.[21] Thus, all other things being equal, higher $N_2(A)$ number densities will lead to higher NO gamma-band excitation rates with consequent increases in gamma band intensity. This may not be the whole story in the present case, however, because for constant $N_2(A)$ number density, larger NO gamma band intensities would also be expected were the NO number density greater at higher pressures. This is likely to be the case since NO is formed from trace impurities of O_2 in the discharge. The mole fraction of this trace impurity should be constant, but its number density will, of course, increase as the total number density in the lamp increases. Thus the increase in the gamma band intensity at higher pressures should result from a combination of higher $N_2(A)$ number densities and higher NO number densities.

The ratio of the HIR to gamma band intensities appears to be relatively constant as pressure is increased. This is another indication that two mechanisms are important in the gamma band intensity increase. Because two $N_2(A)$ molecules are required to produce one $N_2(C'')$ molecule, the HIR intensity should be proportional to the square of the $N_2(A)$ number density. Thus, if the NO number density remained constant, one would expect that the HIR intensity would increase more rapidly than the NO gamma intensity. That it does not is evidence that the NO number density also increases as pressure in the lamp increases.

Figure 6 illustrates the behavior of the three band systems as a function of discharge voltage at a fixed total pressure. All three systems increase quite strongly as the discharge voltage increases. This would be expected since the higher voltages will generate higher number densities of energetic electrons. Note, however, that the NO gamma intensity increases more rapidly than does the intensity of the other two systems as voltage is increased. We think this is because more energy must be expended to produce NO than to excite the electronic states of N_2.

The primary mechanism for NO formation in the discharge will be the reactions of metastable $N(^2D, ^2P)$ with O_2. Thus, in order to generate NO, N_2 must first be dissociated, a process taking almost 10 eV, and then the resultant N atoms must be excited electronically, a process taking another 2.4 to 3.5 eV. At the low electron number densities and energies prevailing in the low-power discharge, relatively little NO will be formed, whereas, as the discharge electrons become more energetic and more numerous, NO formation in the discharge will become much more facile.

4.2.2 Temporal Observations

We gained additional insight on discharge operating characteristics by monitoring the temporal behavior of two different emission features in the discharge region. These experiments used square-wave pulses to power the discharge. A monochromator/photomultiplier combination and 20 MHz digital oscilloscope dispersed, detected, and processed temporal fluorescence signals emanating from the D-B lamp. We monitored two different wavelengths, one corresponding to a normal nitrogen emission in the lamp (N_2 2^+), and the other corresponding to emission from a fragment of a trace impurity that had been added to the lamp. We monitored both wavelengths first before the trace impurity was introduced to the discharge, and then again after its admission.

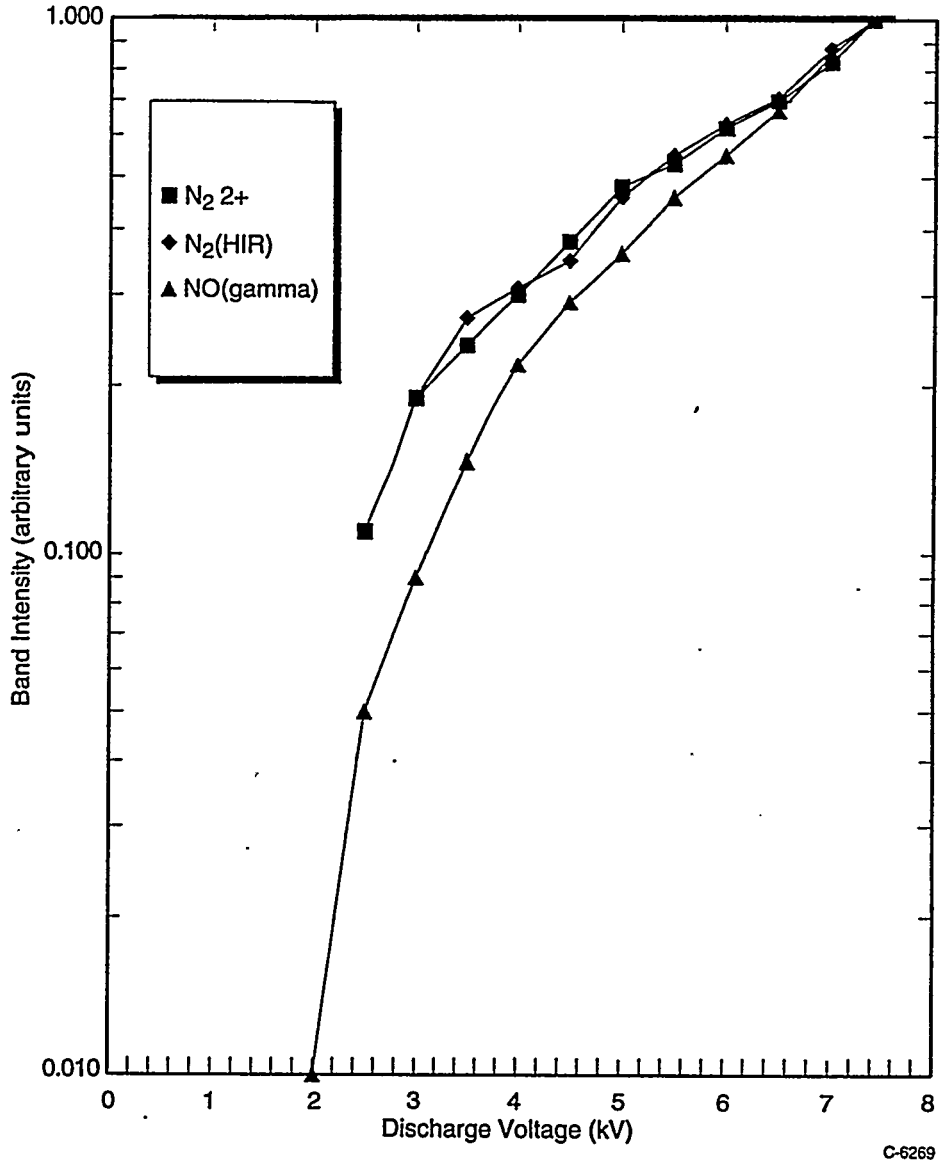

Figure 6. Variation in the relative intensities of the NO gamma bands, $NO(A^2\Sigma^+ - X^2\Pi)$, the nitrogen second-positive bands (2^+), $N_2(C^3\Pi_u - B^3\Pi_g)$, and the nitrogen Herman infrared (HIR) bands, $N_2(C''^5\Pi_u - A'^5\Sigma_g^+)$, as a function of discharge voltage in an N_2 D-B discharge operating at about 700 Torr.

The species used in these studies was 1,1-difluoroethane. Its presence in the discharge is signaled by emission from CN at 387 nm. The N_2 2^+emission band was at 380 nm.

Figures 7 and 8 summarize our results. Figure 7 shows the emissions at the two wavelengths before $C_2H_4F_2$ was added to the lamp, and in addition, the output from a monitor on the pulsing circuit. The pulse is a square wave, and the emissions occur in two short spikes during each cycle of the voltage pulse driving the discharge. The apparent width of the spikes is less than 50 μs. The temporal behavior of the emissions at both wavelengths is essentially identical.

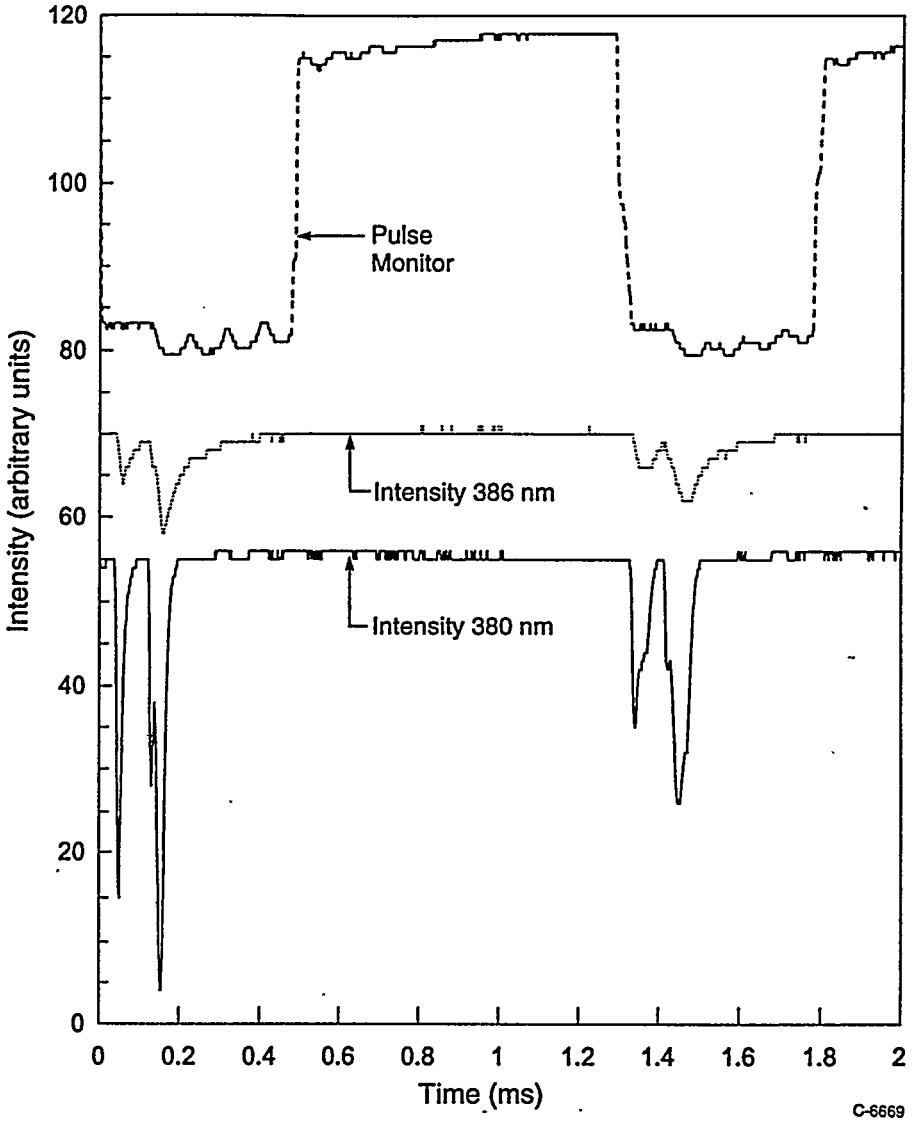

Figure 7. Temporal history of emissions at 380 and 386 nm in a D-B discharge compared to the timing of the discharge pulse driver when no $C_2H_4F_2$ has been added to the discharge.

Figure 8 shows the two emissions after traces of $C_2H_4F_2$ were admitted to the lamp. The temporal behavior of the emission at 380 nm is virtually the same as those in Figure 7. The 387-nm emission, on the other hand is much stronger, and also extends over a much longer time period. Significant emission is still evident more than 500 μs after initiation of the discharge pulse.

These results are an additional indication of nitrogen metastable production in the D-B discharge, and help confirm the ANET excitation mechanism. In the absence of the organic contaminant, lamp emissions are those excited by direct electron impact in the lamp. The nitrogen state emitting at 380 nm has a radiative lifetime of about 40 ns, so its temporal behavior in the discharge is a reflection of the duration of the discharge itself, or more likely in the present case, the temporal resolution of the detection electronics. This resolution is on the order of 10 μs.

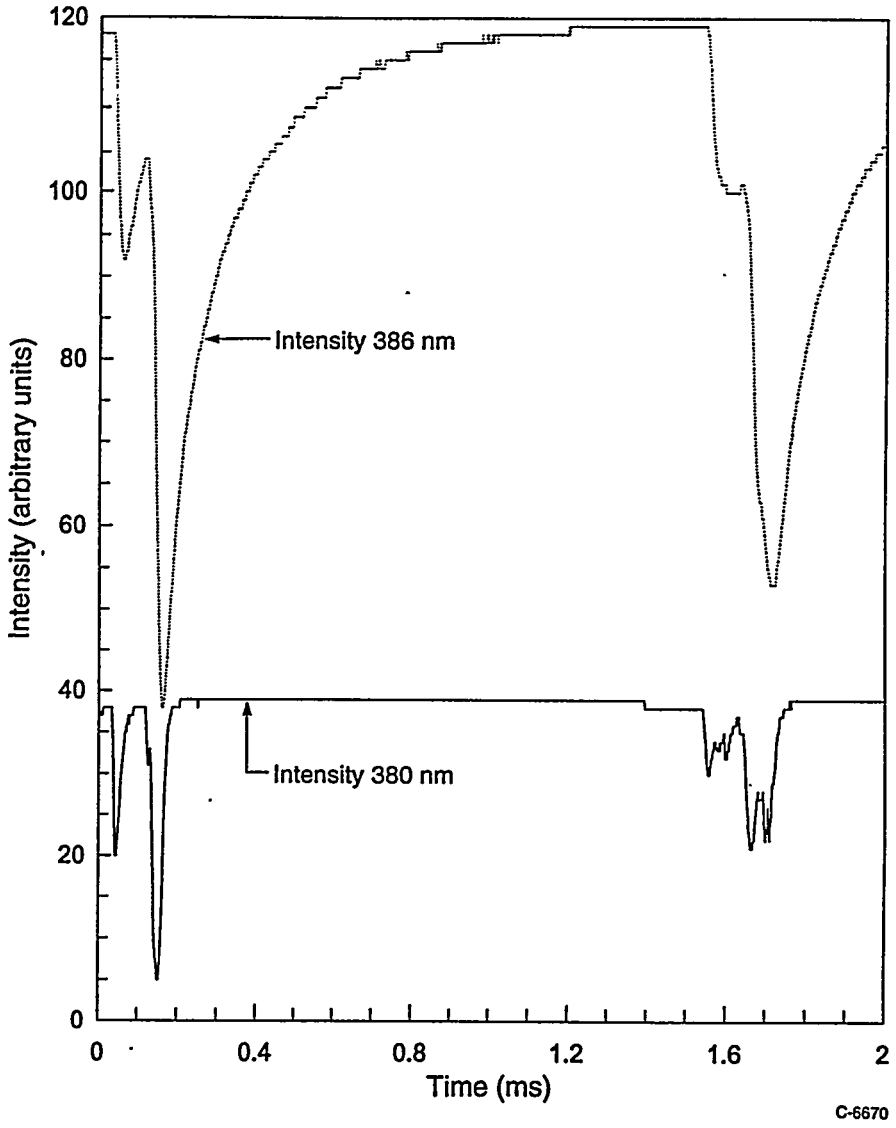

Figure 8. Temporal history of emissions at 380 and 386 nm in a D-B discharge when $C_2H_4F_2$ has been added to the discharge.

When small quantities of the organic molecule are added to the discharge, however, they will be excited by energy transfer from nitrogen metastable molecules. The temporal behavior of the short-lived CN state (60 ns)[24] excited by the metastables will reflect the relaxation time of the metastables themselves. Because the metastable-nitrogen radiative lifetime is quite long (2.5 s),[17] its lifetime after creation in the discharge is determined by collisional effects, i.e., quenching. This quenching can be by the admitted contaminant species if it is abundant enough, by some other species admitted with the hazardous material being analyzed, e.g., oxygen, or by the atmospheric-pressure nitrogen in the discharge.

We can obtain an estimate of the metastable lifetime in the discharge, under the conditions of the experiments, if we plot the decay of the 387-nm emission trace in Figure 8 in semi-logarithmic form and then compute the resulting slope. Such a plot is shown in Figure 9, where we have plotted the natural log of the decay and for comparison a straight-line fit to the data between 250 and 840 μs. The lifetime computed from the slope of the fit indicated in Figure 9 is about 230 μs. The rate coefficient for metastable nitrogen $N_2(A)$ quenching by N_2 is about 3×10^{-16} cm^3 $molecule^{-1}$ s^{-1}. This translates to a quenching lifetime of about 150 μs for a nitrogen quencher at 750 Torr, a value in reasonable accord with our temporal measurement. We thus have additional support for the ANET excitation process.

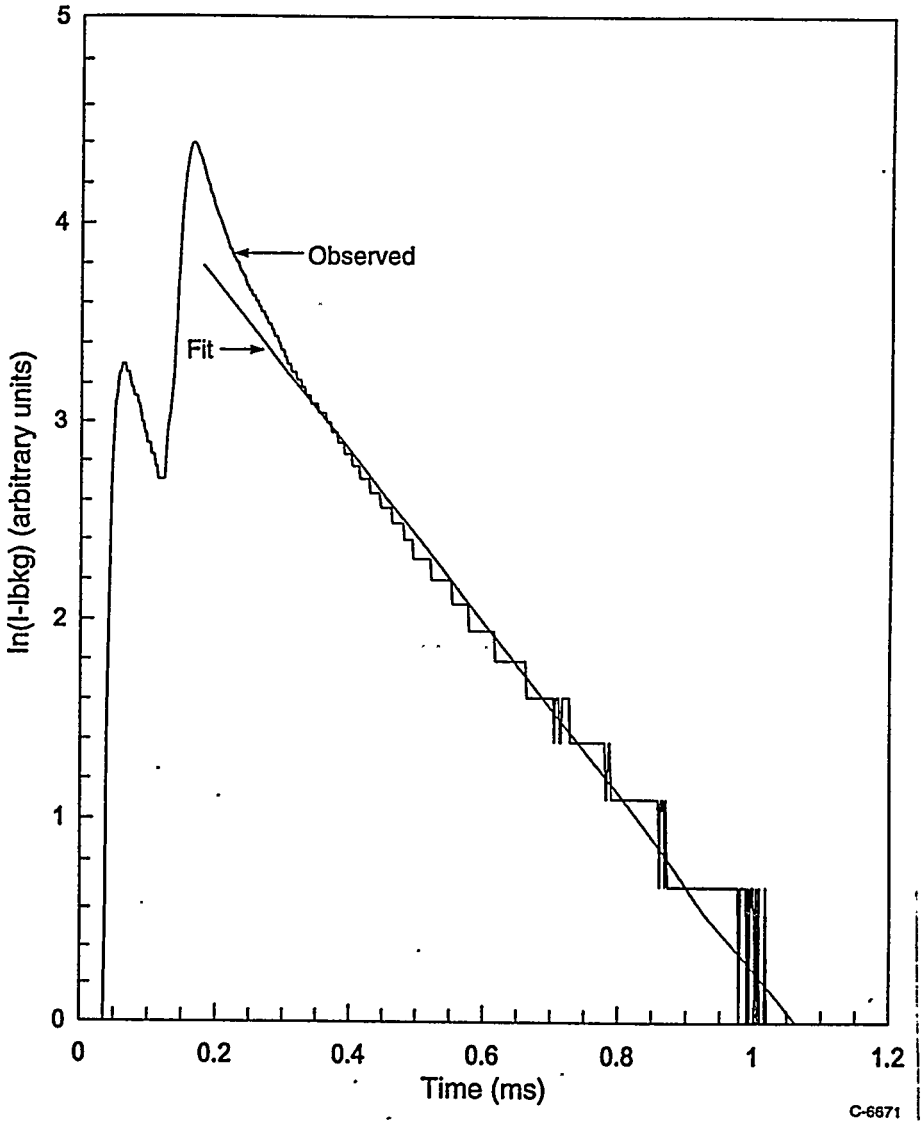

Figure 9. Semi-log plot of the decay of emission at 387 nm.

4.2.3 Observations of Metastable Quenching

In order to understand how the metastable number densities in the discharge region varied as small quantities of metastable quenching species were added to the discharge, we investigated

how the N_2 Herman infrared (HIR) bands varied in intensity as we added several different quenchers. Because metastable quenching can strongly affect the ultimate sensitivity of our approach, it is vitally important to understand this quenching in some detail. Some readers might find the following a bit tedious, and may prefer to jump ahead to Subsections 4.3 through 4.6 where we present our results on the identification of spectral features characteristic of different hazardous materials and sensitivity limits for their detection.

A number of years ago we demonstrated that the HIR system is excited in an energy-pooling reaction between two metastable nitrogen molecules, $N_2(A\,^3\Sigma_u^+)$[23]. The metastables, each of which have about 6 eV internal energy combine their energies to generate one nitrogen molecule with an internal energy about 11 eV, and one ground electronic state molecule. As a result, the HIR system, which is much easier to observe than the highly forbidden Vegard-Kaplan bands, $N_2(A\,^3\Sigma_u^+ -- X\,^1\Sigma_g^+)$, can provide a diagnostic test for the presence of nitrogen metastables in a D-B discharge.

This system provides a superior diagnostic to the often used NO gamma bands, $NO(A^2\Sigma^+ -- X\,^2\Pi)$, which are also excited by metastable energy transfer to NO[21]. Nitric oxide is formed in discharge-induced reactions involving small oxygen impurities in the nitrogen that makes up the bulk of the discharge gas. Thus, variations in impurity concentrations will affect its number density, and thereby the intensity of NO gamma-band fluorescence. The HIR system, on the other hand, depends *only* upon nitrogen metastable number densities.

We investigated HIR spectra emitted by the lamp as a function of added quencher. For these experiments we used a mixture of 5% O_2, 0.2% SO_2, and the balance N_2. Because the rate coefficient for $N_2(A)$ quenching[9] by SO_2 is about ten times that for quenching by O_2, the experiments are equivalent to using a 7% mixture of O_2. We also investigated quenching by CO_2.

Figure 10 shows the spectrum of the lamp emission between 650 and 900 nm. The gas in the lamp was nitrogen at a pressure of about 700 Torr. By far the strongest features in the spectrum are the Herman Infrared bands. The nitrogen first-positive bands, $N_2(B\,^3\Pi_g -- A\,^3\Sigma_u^+)$ appear only weakly because the $N_2(B)$ state is strongly quenched by molecular nitrogen[22]. For the quenching experiments, we confined out spectral observations to the region between 675 and 715 nm. The delta v=2 sequence of the HIR bands are centered in this spectral region. A small portion of the delta v=3 sequence of the first-positive system from v'=4 and 3 is included at the short wavelength end of the spectral region while bands from the delta v=2 sequence with $v' \geq 6$ are at the long wavelength end. The first-positive bands that overlap with the HIR bands are so weak as to be unobservable, and therefore of no consequence in the present study. One interesting feature of the spectrum in Figure 10 is the presence of emission from v'=4 of the HIR system. To our knowledge bands from this upper level have not been reported previously.

Figure 11 shows how the intensities of the first-positive and HIR bands between 675 and 715 nm change as small amounts of the quenching gas mixture are added to the discharge gas. The addition of the quench gas causes a rapid decrease in the intensities of the HIR bands relative to the first-positive bands. Although it is not obvious in Figure 11, emission from v'=4 of the HIR system is quenched much less efficiently than the other two vibrational levels observed. We

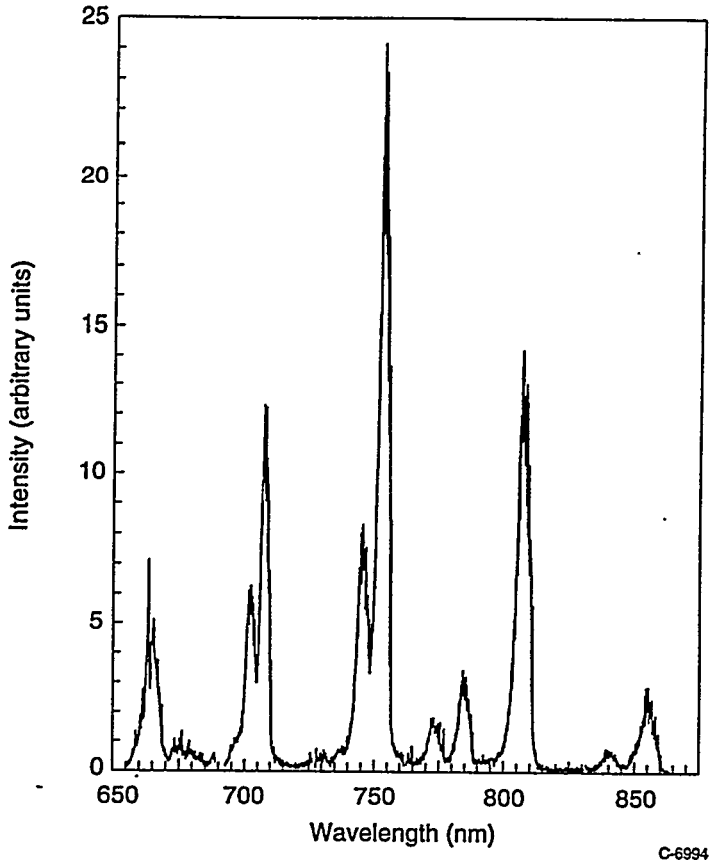

Figure 10. Spectrum of N_2 Herman infrared emission in a dielectric-barrier discharge at 700 Torr.

believe that these observations can be explained if the first-positive bands are excited primarily by electron impact but that the HIR emissions from v'=2 and 3 are excited primarily by metastable $N_2(A)$ energy pooling reactions.

We analyze our data using the following reaction set:

$$N_2 + e^- \rightarrow N_2(A\ ^3\Sigma_u^+) + e^- \quad \text{(1a)}$$

$$N_2(B\ ^3\Pi_g) + e^- \quad \text{(1b)}$$

$$N_2(C''\ ^5\Pi_g) + e^- \quad \text{(1c)}$$

$$N_2(A) + N_2 \rightarrow 2\ N_2 \quad \text{(2a)}$$

$$N_2(B) + N_2 \rightarrow 2\ N_2 \quad \text{(2b)}$$

$$N_2(C'') + N_2 \rightarrow 2\ N_2 \quad \text{(2c)}$$

$$N_2(A) + O_2 \rightarrow N_2 + O_2 \quad \text{(7a)}$$

$$N_2(B) + O_2 \rightarrow N_2 + O_2 \quad \text{(7b)}$$

$$N_2(C'') + O_2 \rightarrow N_2 + O_2 \quad \text{(7c)}$$

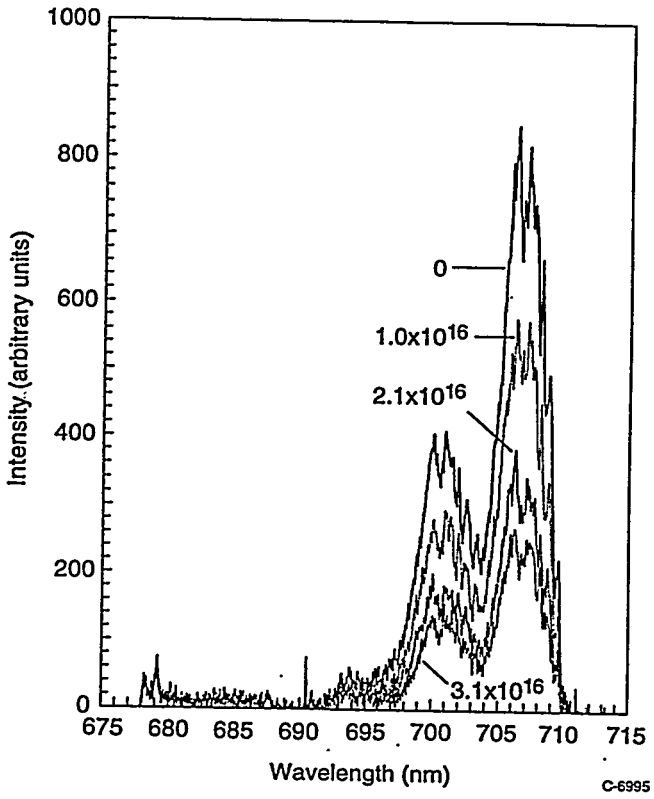

Figure 11. Spectrum of the $\Delta v=2$ sequence of the N_2 Herman infrared system in a D-B discharge in the absence of trace additions of a quenching gas mixture, and with three different concentrations of the quenching gas added.

$$N_2(A) + N_2(A) \rightarrow N_2(C'') + N_2(X) \quad (10a)$$

$$N_2(B) + N_2(X) \quad (10b)$$

$$N_2(B) \rightarrow N_2(A) + h\upsilon \text{ (first-positive bands)} \quad (11a)$$

$$N_2(C'') \rightarrow N_2(A') + h\upsilon \text{ (HIR bands)} . \quad (11b)$$

Approximate rate coefficients for reactions 2b and 7b are 3×10^{-11} and 2×10^{-10} cm^3 $molecule^{-1}$ s^{-1}, respectively[22]. Because the nitrogen number density in our experiments is about 2×10^{19} molecules cm^{-3} or greater and the maximum number density of O_2 is only 3×10^{15} molecules cm^{-3}, $N_2(B)$ quenching by O_2 will be negligible and we can ignore reaction 7b in our further analysis. To our knowledge, no rate coefficients have been determined for quenching of $N_2(C'')$ although some experimental evidence suggests that this state is removed more efficiently by radiation than by quenching at pressures on the order of a few Torr. For our analysis we shall assume that losses of $N_2(C'')$ by radiation and quenching by N_2 dominate that from quenching by O_2. In this case, such quenching will not vary with small added amounts of O_2. Radiative removal of $N_2(A)$ is entirely negligible compared to removal due to nitrogen and impurity quenching.

The differential equation describing the temporal behavior of $N_2(A)$ is

$$d[N_2(A)]/dt = k_{1a}[N_2][e^-] - (k_{2a}[N_2] + k_{7a}[O_2])[N_2(A)] . \quad (12)$$

Because we are observing the average intensities resulting from a number of repeated discharge pulses, we can treat $N_2(A)$ as if it were in steady state. Thus the effective $N_2(A)$ number density is

$$[N_2(A)] = k_{1a}[N_2][e^-]/(k_{2a}[N_2] + k_{7a}[O_2]) . \quad (13)$$

Similarly, we can derive the effective number densities of $N_2(B)$ and $N_2(C'')$ to be

$$[N_2(B)] = k_{1b}[N_2][e^-]/(k_{11a} + k_{2b}[N_2]) \quad (14)$$

and

$$[N_2(C'')] = \{k_{1c}[N_2][e^-] + k_{10a}[N_2(A)]^2\}/\{k_{11b} + k_{2c}[N_2]\} . \quad (15)$$

We observed that the intensity of the $N_2(B)$ levels monitored remained relatively constant as quencher was added to the discharge. We take this as an indication that k_1 is the only important populating mechanism for formation, i.e. any possible contribution from reaction 10b can be ignored. Furthermore, we infer that the basic electron-impact excitation process is unaffected by the addition of small amounts of quencher. If $N_2(B)$ excitation is essentially constant, then it is reasonable to assume that such will also be the case for electron-impact excitation of $N_2(A)$. We use this assumption in our subsequent analysis. The fact that our analysis yields reasonable results, lends support to our having made it.

We have indicated that the $N_2(C'')$ state has two formation mechanisms, electron impact excitation and metastable energy pooling. Because the energy of $N_2(C'')$ state is almost double that of the $N_2(A)$ state, and because the $N_2(C'')$ state is not readily observed in nitrogen discharges under most conditions, we expect that the electron-impact component is negligible compared to the metastable energy-pooling component. We thus ignore the electron-impact component in our subsequent analysis. With this assumption, we can rearrange Eq. (15) to get

$$\{((k_{11b} + k_{2c}[N_2])/k_{10a})[N_2(C'')]\}^{1/2} = [N_2(A)] . \quad (16)$$

Combining this result with Eq. (13) gives

$$\{1/[N_2(C'')]\}^{1/2} = \kappa(k_{2a}[N_2] + k_{7a}[O_2]) \quad (17)$$

where κ is effectively constant at constant pressure and is given by

$$\kappa = \{(k_{11b} + k_{2c}[N_2])/k_{10a}\}^{1/2} / k_{1a}[N_2][e^-] . \quad (18)$$

Figures 12 and 13 show how the reciprocal of the square root of the HIR intensity (proportional to $[N_2(C'')]$) varies as a function of added $[O_2]$, for $N_2(C'')$ in vibrational levels 2 and 3 respectively, at four different total lamp pressures. The data sets have been offset for clarity.

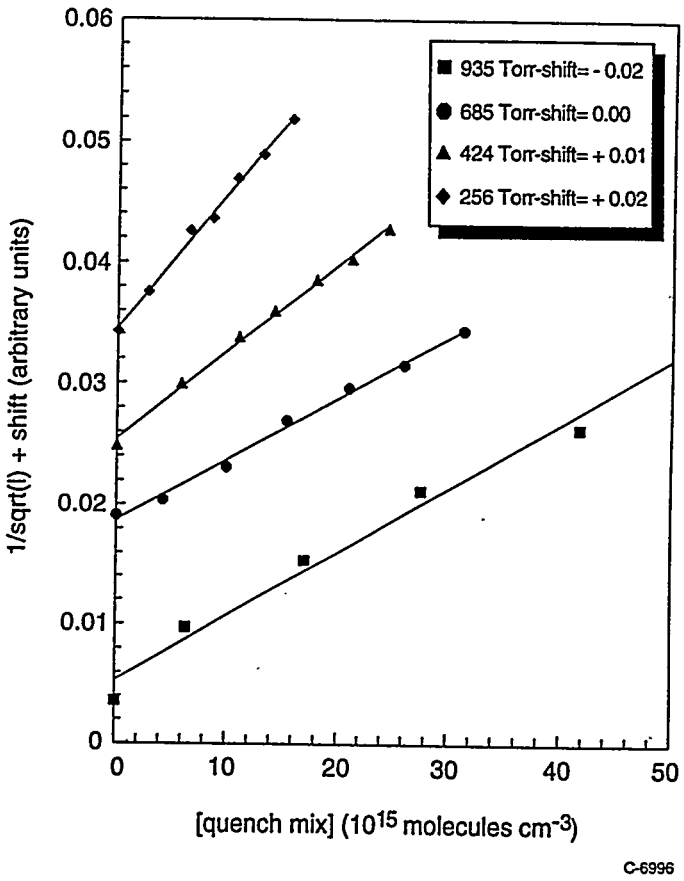

Figure 12. Stem-Volmer plot of metastable quenching in a D-B discharge as determined from fluorescence intensity measurements of the v'=2 to v''=0 band of the N_2 Herman infrared system at four different total N_2 pressures in the D-B lamp.

The ratio of the slope to intercept of the best-fit lines in Figures 12 and 13 gives the ratio of the rate coefficient for $N_2(A)$ quenching by O_2 to the rate of $N_2(A)$ removal by nitrogen quenching. These ratios vary with total pressure, being larger at higher pressures where the nitrogen quenching is relatively more important. If we plot these ratios as a function of total pressure, we can obtain an estimate of the rate coefficient for oxygen quenching to that for nitrogen quenching. Such a plot is shown in Figure 14. After correction for the fraction of active quencher in the quenching gas mixture, the slopes of the lines in Figure 14 give the rate-coefficient ratios, 1.1 and 1.3 x 10^{-4} for v'=2 and 3 respectively.

Under conditions where only low vibrational levels of $N_2(A)$ are present, $N_2(C'', v'=3)$ is formed almost exclusively by energy pooling between two $N_2(A, v'=0)$ molecules while $N_2(C'', v'=2)$ is formed in collisions between $N_2(A, v'=0)$ and $N_2(A, v'=1)$[23]. The rate coefficients for O_2 quenching of $N_2(A)$ is 2.3 and 4.1 x 10^{-12} cm^3 $molecule^{-1}$ s^{-1}, for $N_2(A, v'=0)$ and $N_2(A, v'= 1)$,

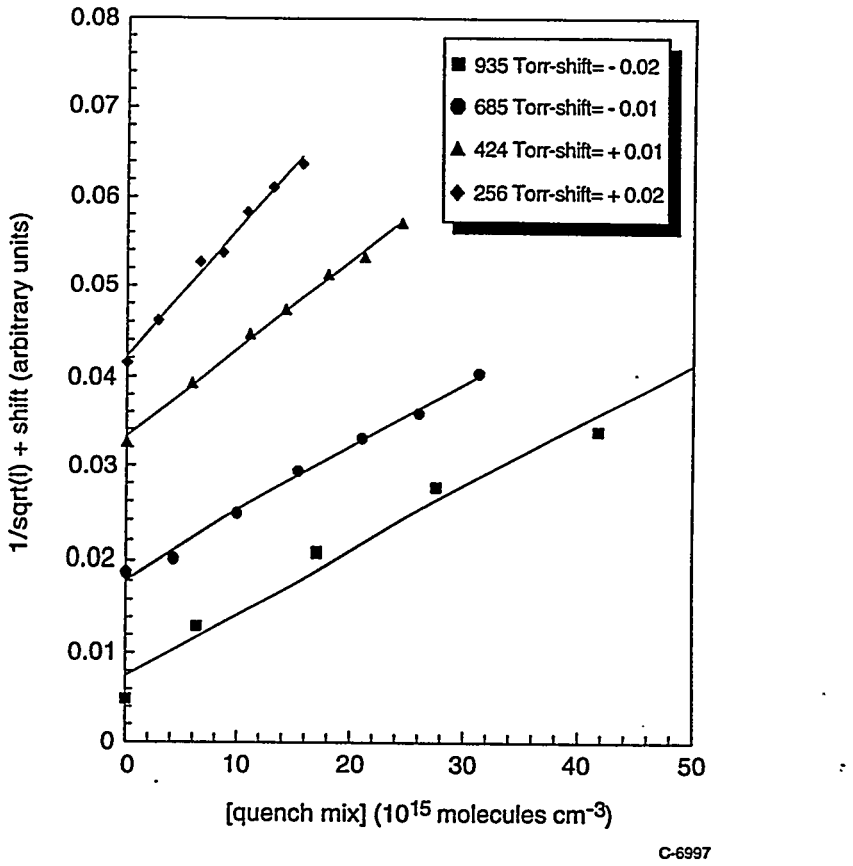

Figure 13. Stern-Volmer plot of metastable quenching in a D-B discharge as determined from fluorescence intensity measurements of the v'=3 to v"=0 band of the N_2 Herman infrared system at four different total N_2 pressures in the D-B lamp.

respectively[19]. Taking an average value of 3.2×10^{-12} cm^3 $molecule^{-1}$ s^{-1} for the combination of $N_2(A)$ v'=0 and 1, the data for $N_2(C'', v'=2)$ indicates a value for k_{2a} of 3.5×10^{-16} cm^3 $molecule^{-1}$ s^{-1} while that for $N_2(C'', v'=3)$ implies a k_{2a} of 3.0×10^{-16} cm^3 $molecule^{-1}$ s^{-1}.

The values just determined for k_{2a}, agree excellently with the measurement of Dreyer and Perner[18] 3.5×10^{-16} cm^3 $molecule^{-1}$ s^{-1}, but are substantially above Levron and Phelps' values of 2.0×10^{-18} and 4.3×10^{-18} cm^3 $molecule^{-1}$ s^{-1}, for vibrational levels 0 and 1, respectively[25]. We think under the present conditions the comparison with the Dreyer and Perner results are more meaningful. Levron and Phelps took extraordinary precautions to ensure that their nitrogen was free from even minute traces of contaminants. We did not, nor do Dreyer and Perner appear to have done so. Thus our measurement and theirs is essentially a determination of quenching by nitrogen and/or the minute traces of contaminants that routinely inhabit high purity nitrogen, typically a few parts per million of O_2, hydrocarbons, and moisture.

We think that our good agreement with the data of Dreyer and Perner, therefore lends considerable credence to our contention that the HIR system is populated by metastable energy pooling, and justifies the various approximations and assumptions we have made in our analysis. We also note that the temporal analysis of metastable-excited fluorescence given above is consistent with the value of the rate coefficient for metastable quenching by N_2 determined here.

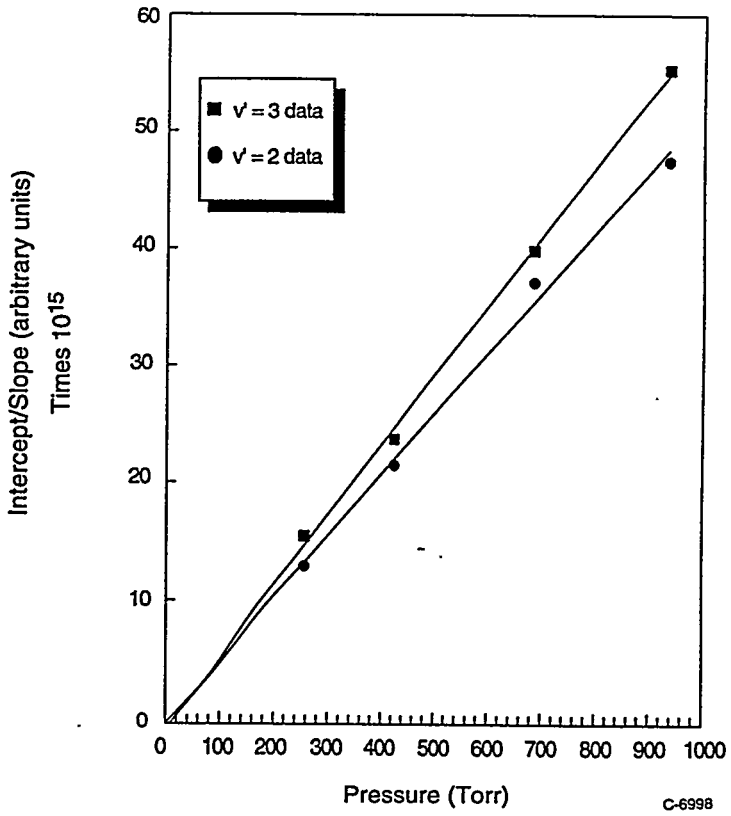

Figure 14. Plot of the ratios of the intercepts to slopes of the lines in Figures 12 and 13 as a function of total lamp pressure.

4.3 Heavy Metal Detection

Our studies on heavy metal detection focussed primarily upon mercury detection. In addition to mercury, however, we our results also demonstrate sensitive detection of Cr and Se. We begin first with our experiments on mercury. They include not only observations on mercury excitation in the D-B discharge, but also measurements of mercury fluorescence quenching and observations that ANET can be used to distinguish $HgCl_2$ from free Hg. We then follow with our experiments on Cr and Se.

For these experiments, we used volatile compounds. The purpose of this was to allow easier determination of the best wavelengths to monitor for each element, and enhance the accuracy of quantitative detection limit determinations.

4.3.1 Detection of Elemental Mercury

Only one new emission feature is observed when Hg was added to N_2* produced in the D-B lamp, the 253.7 nm line from $Hg(6^3P_1)$. Figure 15 shows the spectral region in the vicinity of the Hg 253.7 nm emission line. The mercury line is prominent in the spectrum and is near, but well separated from, a band of the $NO(A^2\Sigma^+ - X^2\Pi)$ system. These bands are also excited by energy transfer from metastable nitrogen.[22] The NO is formed in the discharge in reactions involving traces of oxygen in the nitrogen.

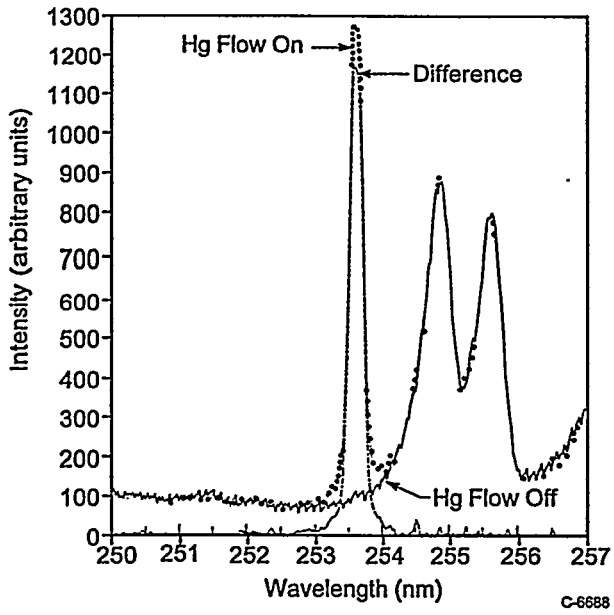

Figure 15. Spectrum of dielectric-barrier discharge in the presence and absence of about 0.14 ppt added Hg and the difference between the two spectra.

Figure 16 shows the spectrum in the vicinity of the mercury line when the NO γ-band background has been subtracted out at four different concentrations of Hg added to the discharge. This illustrates qualitatively that higher Hg concentrations result in larger emission intensities. We determined the integrated emission intensity of the Hg line as a function of Hg mixing ratio in the

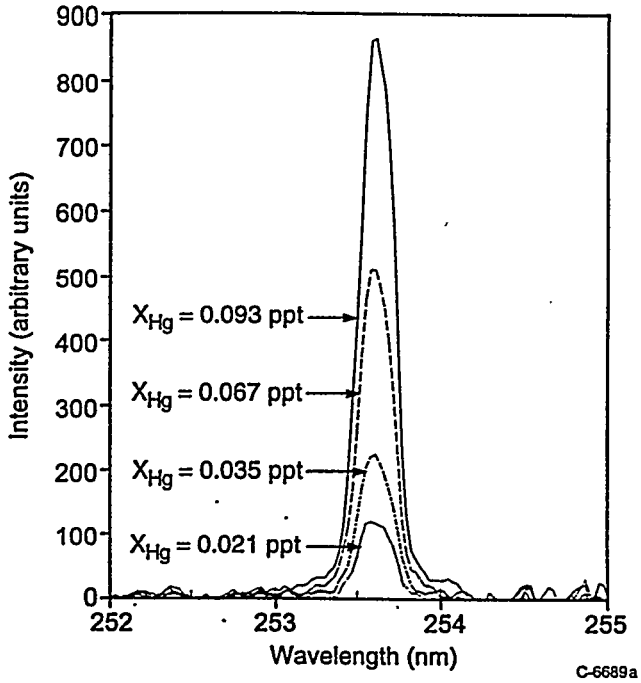

Figure 16. Background-subtracted D-B discharge spectrum Hg at four different Hg mole fractions.

D-B discharge region and have plotted one series of measurements in Figure 17. The abscissa of Figure 17 refers to concentration in terms of parts per trillion on a volume basis in the discharge region. These data can be used to estimate the sensitivity of the ANET technique. Conditions for these measurements were idealized, only Hg and N_2 were in the lamp. The line through the data points indicates the best linear least-squares fit to the data. The slope of the line is about 1×10^7 counts ppb^{-1}. *Taking the conservative approach that a signal of 50 counts is readily observable (S/N ~3, 10 s time constant), we determine a minimum delectability of* 5×10^{-6} *ppb.*

In a practical situation, one may not be able to take samples from a pure nitrogen environment. Thus it becomes important to determine the effects of added species that are likely to accompany the sample. If these species quench the mercury fluorescence, then the sensitivity of ANET will be less than that just established. To learn about this, we monitored the mercury signal from the D-B lamp as a quenching gas mixture was added to the discharge. Our quenching gas was the result of flowing a mixture of 5% CO_2, 10% O_2, 85% N_2 through a cell containing water at ambient conditions. The final mixture thus contained about 3% H_2O.

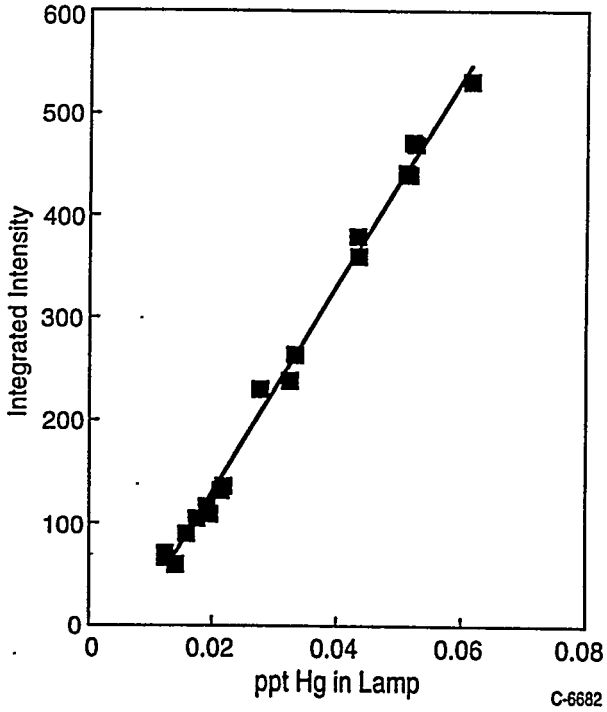

Figure 17. Intensity of Hg 253.7 nm emission excited by ANET as a function of the mole fraction of Hg in a D-B discharge.

Figure 18 shows the results of adding the quenching gas to a D-B lamp containing a constant trace flow of Hg vapor. The Hg signal intensity is plotted in Stern-Volmer fashion, i.e. the reciprocal of the expression in Eq. (8). Such a plot should then be linear in concentration of added quencher if all other conditions remain constant. The slope of the Stern-Volmer plot is

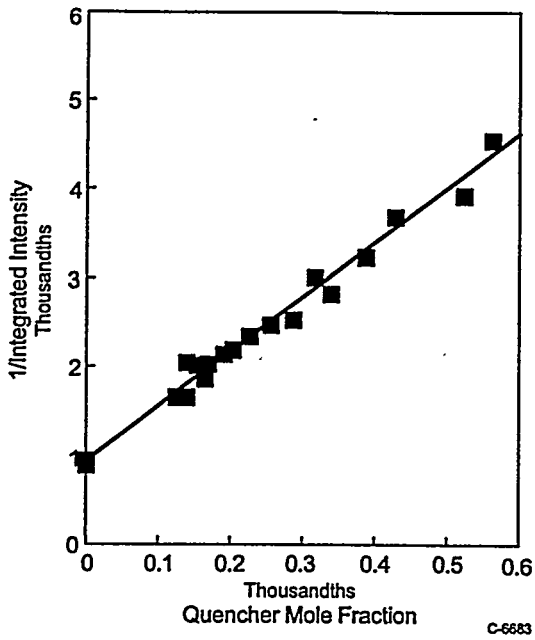

Figure 18. Reciprocal of the intensity of Hg 253.7 nm emission in a D-B discharge as a function of mole fraction of added quenching gas.

proportional to the rate of quenching by the added quencher relative to all other loss processes (e.g., radiation and quenching by the N_2 bath gas). The intercept is proportional to the rate of these other loss processes. As can be seen, the added quench gas does reduce the mercury radiation intensity. The half-quenching mole fraction is the added mole fraction of quencher that reduces the signal level by a factor of 2. It can be computed from the ratio of the intercept in the plot in Figure 18 to the plot's slope. That value is 1.5×10^{-4}. Adding just CO_2 or H_2O to the D-B discharge had a minimal effect on Hg fluorescence intensities. Thus, the quenching is essentially just the result of the presence of O_2 in the gas mix. This means that for a sample in air ($\approx$20% O_2), the half-quenching mole fraction will be further reduced to 7×10^{-5}.

The results from Figures 17 and 18 can be combined to determine an effective sensitivity for detecting mercury in the presence of air. That number will be twice the minimum detectable level under ideal conditions divided by the half-quenching mole fraction. We calculate a value of 0.15 ppb. That means that we will be able to detect mercury levels as low as 0.15 ppb in air even though the sample size is quite small (i.e., about 0.01% of the total gas in the lamp), and in spite of the fact that the air quenches some of the mercury emission.

4.3.2 Detection of Mercuric Chloride

Adding traces of gaseous mercuric chloride to a D-B discharge in nitrogen results in emission from the $HgCl(B^2\Sigma^+ - X^2\Sigma^+)$, as shown in Figure 19. The trap containing the $HgCl_2$ was at room temperature, so its partial pressure in the reagent feed was only 1.3×10^{-4} Torr. Thus, the $HgCl_2$ was admitted at ppb levels. Nevertheless, the spectrum is quite strong and readily assigned. An interesting feature in the spectrum is that one can distinguish emission from $Hg^{37}Cl$ as well as $Hg^{35}Cl$. Thus in this instance, the ANET approach can be used to quantitate isotopic ratios. We did not make quantitative measurements of our system's sensitivity for $HgCl_2$ detection, but based upon the small amount sampled, it must be at ppb levels if not better.

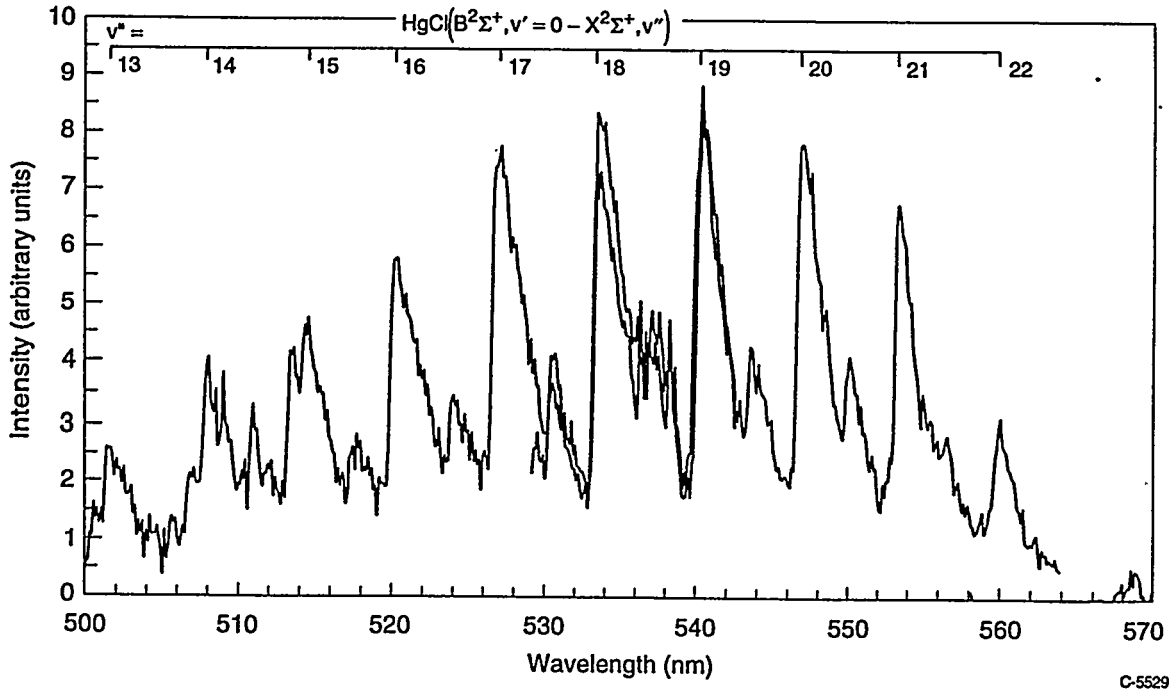

Figure 19. Spectrum of dielectric barrier discharge in N_2 at atmospheric pressure in the absence and presence of added $HgCl_2$.

4.3.3 Detection of Chromium

Figure 20 shows the spectra generated in the D-B lamp in the absence of any added chromium compound, with traces of a chromium compound added, and the difference between the two spectra, which is a spectrum of just the Cr emission. ANET also excites chromium weakly between 357 and 360 nm (see Figure 21). This illustrates the selective nature of ANET because in an arc, the lines in both spectral regions are of comparable intensity.

Pure Cr spectra in the 425 nm region, at four different added mole fractions, are plotted in Figure 22, again confirming that emission intensities increased as the Cr mole fraction increased. We measured the integrated intensities of the Cr emission as a function of Cr compound number density in the D-B lamp. Figure 23 shows the results of the experiments. The solid line in Figure 23 is the least-squares best fit to the data.

We can estimate the overall sensitivity of our system from the analysis of the data in Figure 23. The slope of the best-fit line is about 0.75 counts ppb^{-1}. Under the conditions of the experiments, a signal of 50 counts would have been readily observable, which would have been produced by having a mixing ratio of about 35 ppb in the discharge region. Combining this result with the metastable half-quenching mole fraction for air, determined above in Subsection 4.2.3 allows an estimate of the chromium detection sensitivity in air. The half quenching mole fraction was about 5×10^{-4}. This would imply a detection sensitivity of about 70 ppm. This value isn't particularly good, and not really believable given the extraordinary sensitivity ANET has shown in other situations, and the extraordinary efficiency metastable nitrogen excitation generally manifests. We think that our estimate of the vapor pressure of the chromium compound used in

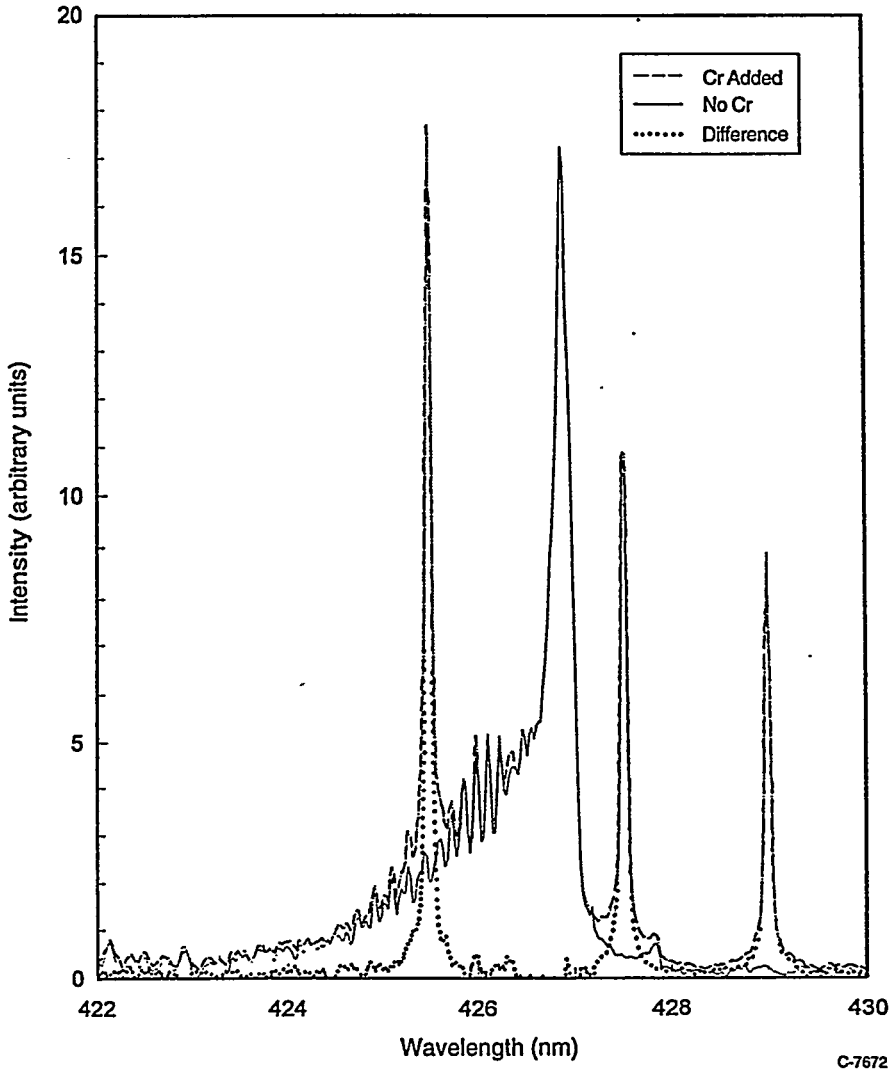

Figure 20. Spectrum of a dielectric-barrier discharge lamp in nitrogen at atmospheric pressure in the absence of any added Cr compound, with 1 part per million of added Cr compound, and the difference between the two spectra.

the experiments must be seriously in error. In keeping with this, one would expect that additive concentrations at the levels calculated ought to have a significant quenching effect on background emissions in the lamp. In fact the background emissions were essentially invariant over the range of added compound. Thus we think that the vapor pressure must have been substantially below that calculated. We hope to resolve this discrepancy in future work.

4.3.4 Detection of Selenium

Figures 24 and 25 show the spectra between 189 and 209 nm generated in the D-B lamp in the absence of any added selenium compound, with traces of a selenium compound added, and the difference between the two spectra, which is a spectrum of just the Se emission. The Se concentration in Figure 24 was about 0.024 parts per billion (ppb), while that in Figure 25 was

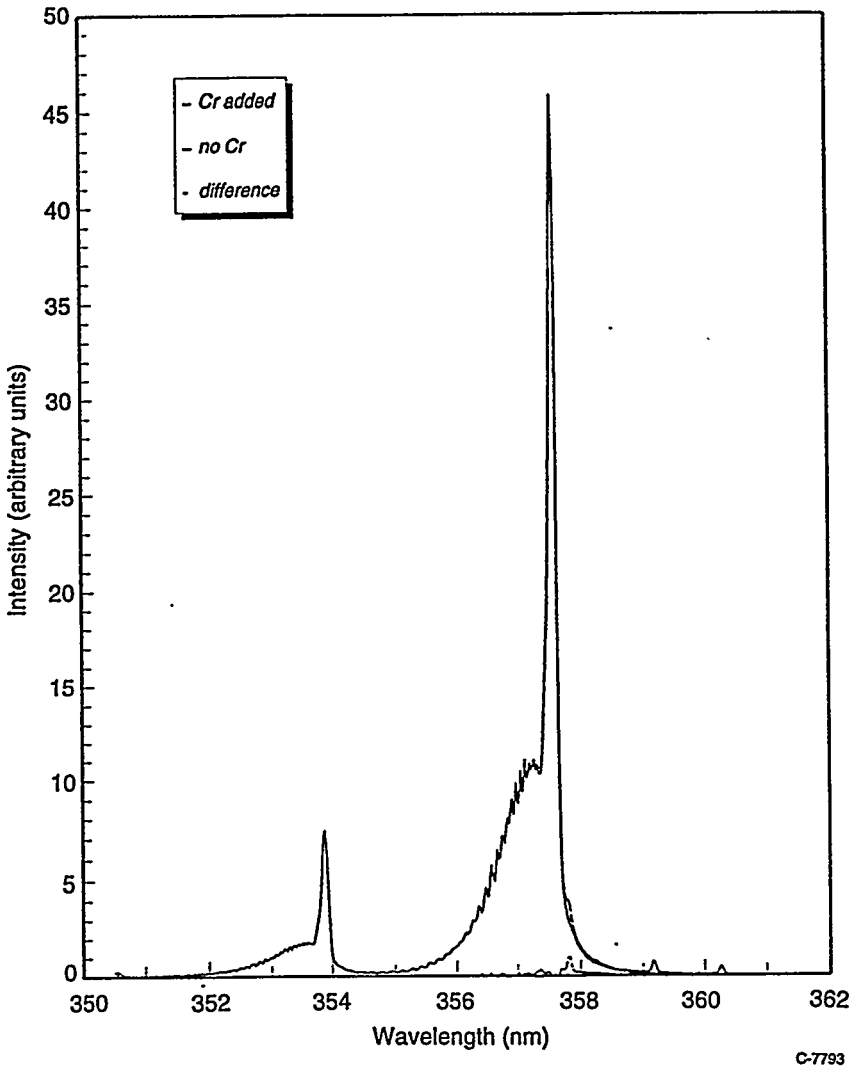

Figure 21. Atomic Cr emissions ~ 357 to 360 nm excited in the D-B discharge.

0.50 ppb. At the lowest concentration, only the line at 207.5 nm is clearly apparent, whereas at the higher concentration, the 196.0, 204.0, and 206.5 nm triplet is in evidence.

Figure 26 shows the spectral region between 202 and 220 nm for a Se concentration of 0.036 ppb. In addition to the strong 207.5 nm line, another fairly strong line appears at 216.5 nm, while the 204.0 nm line is barely discernable. These spectra illustrate one of the interesting features of ANET excitation. In an arc source, the shorter wavelength triplet emission is well over an order of magnitude stronger than the longer wavelength doublet. The specificity of ANET excitation, however, reverses the situation quite dramatically. Note also that the 207.5 nm transition is well isolated from background emissions in the spectrum, so that one should expect to detect it with considerable sensitivity.

Pure Se spectra at five different added mole fractions are plotted in Figure 27. We see that as with the other heavy metals studied, larger Se concentrations result in greater emission

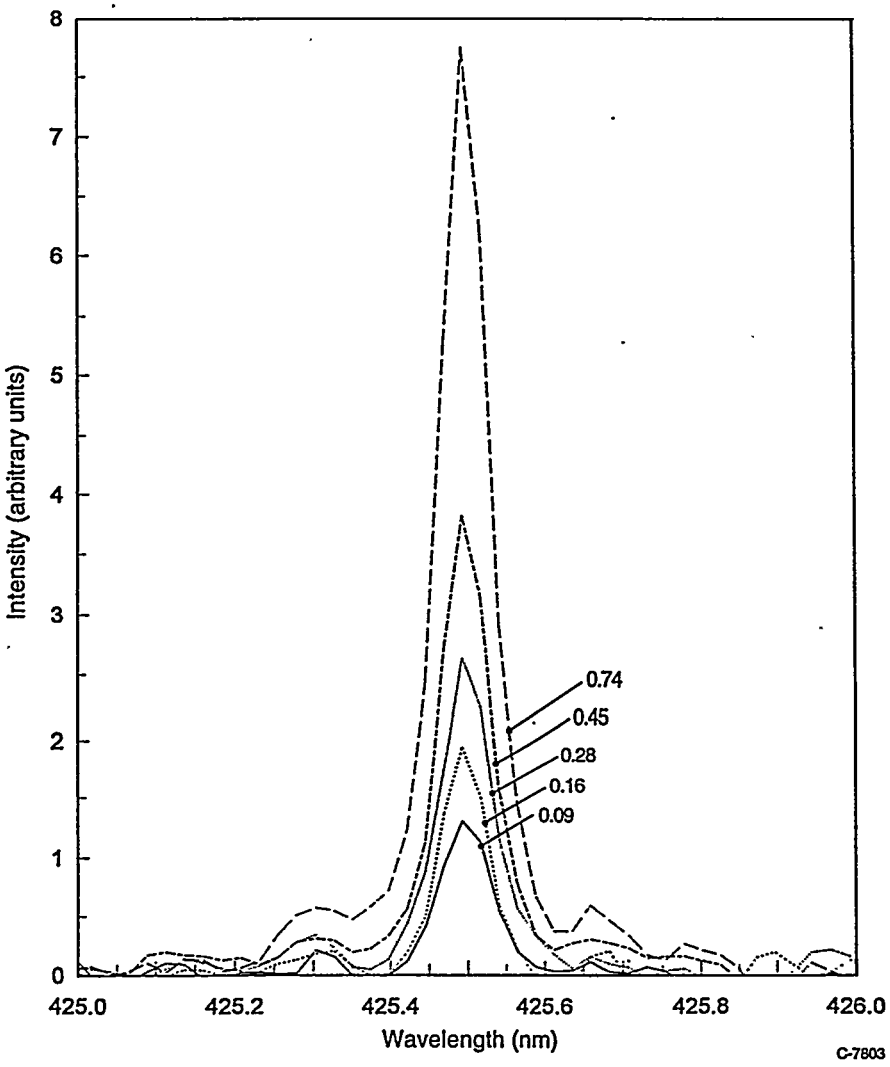

Figure 22. Difference spectra of D-B discharge lamp in atmospheric pressure nitrogen at four different added mole fractions of a Cr compound.

intensities. We measured the integrated intensities of the Se emission as a function of Se compound number density and have plotted the results in Figure 28. The solid line in Figure 8 is the least-squares best fit to the data. The slope of the best-fit line is about 7.2×10^4 counts ppb^{-1}. Under the conditions of the experiments, a signal of 50 counts would have been observable with a signal-to-noise ratio of about 1:1. This signal would have been produced by having a mixing ratio of about 7×10^{-4} ppb in the discharge region.

In order to estimate a selenium detection sensitivity under conditions where the sample will be taken in air, we need to correct the above value for quenching and sample dilution. The metastable quenching data described in Subsection 4.2.3 indicate a half quenching mole fraction for air of about 5×10^{-4}. Thus in air we expect a detection sensitivity for Se of about 0.7 ppb.

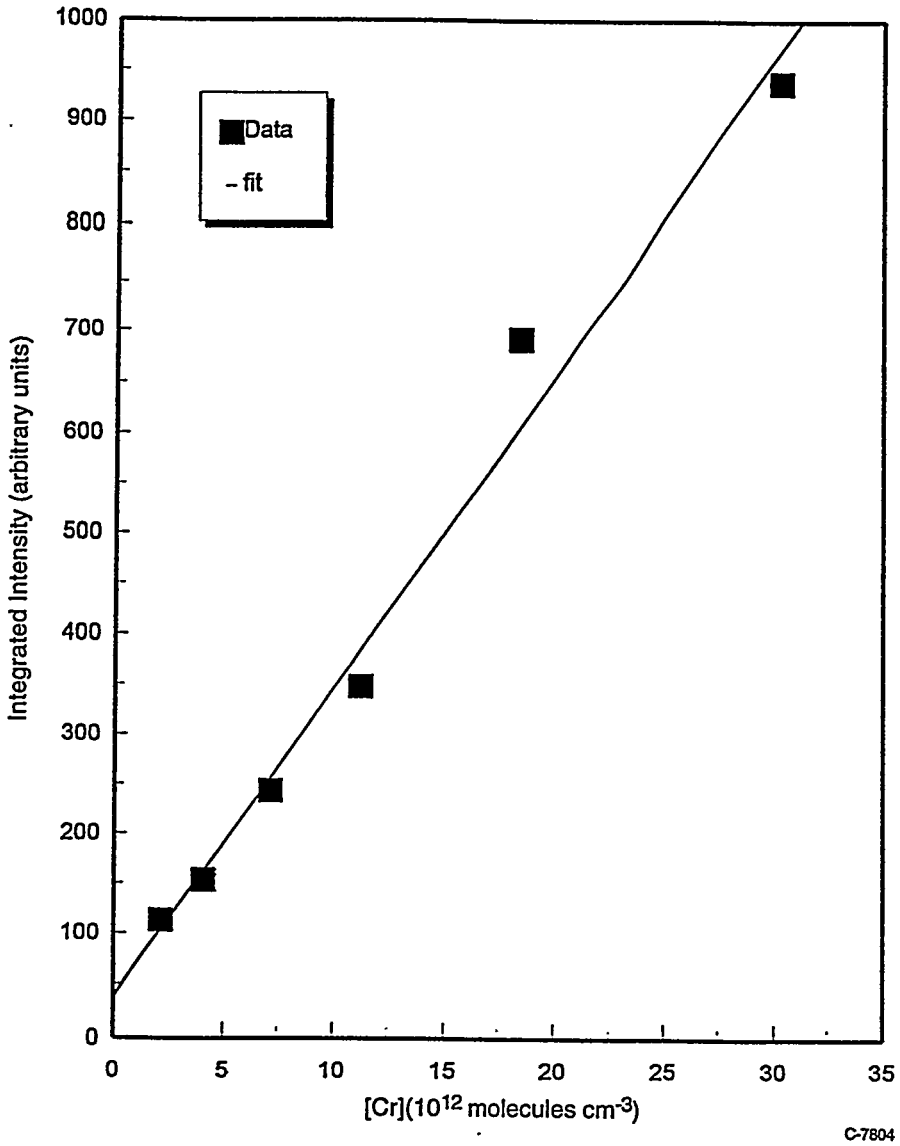

Figure 23. The integrated intensity of the Cr line at 425.4 nm as a function of the number density of a Cr compound added to an atmospheric pressure N_2 lamp.

Selenium is one of the more difficult elements to detect by conventional means. The most widely used techniques, flame AA (atomic absorption) and ICP-OES (inductively coupled plasma excitation combined with optical emission spectroscopy) have sensitivity limits of about 70 and 60 ppb, respectively[1]. We thus see, that ANET, even though a very simple technique, has great potential as a sensitive analytical technique.

4.4 Detection of Organic Compounds

During the course of this phase of the program we investigated the ANET spectra excited when a number of different organic molecules were added to the D-B discharge. Molecules studied included 1,1-difluoroethane, 1,2-dichloroethane, 1-chlorobutane, trichloroethylene, chloroform, hexane, methyl alcohol, iso-propyl alcohol, acetone and bromo-trifluoromethane. In all instances, adding organic compounds in trace amounts to the atmospheric-pressure D-B discharge in nitrogen resulted in strong CN($B^2\Sigma^+$ -- $X^2\Sigma^+$) emission around 388 and 420 nm. In

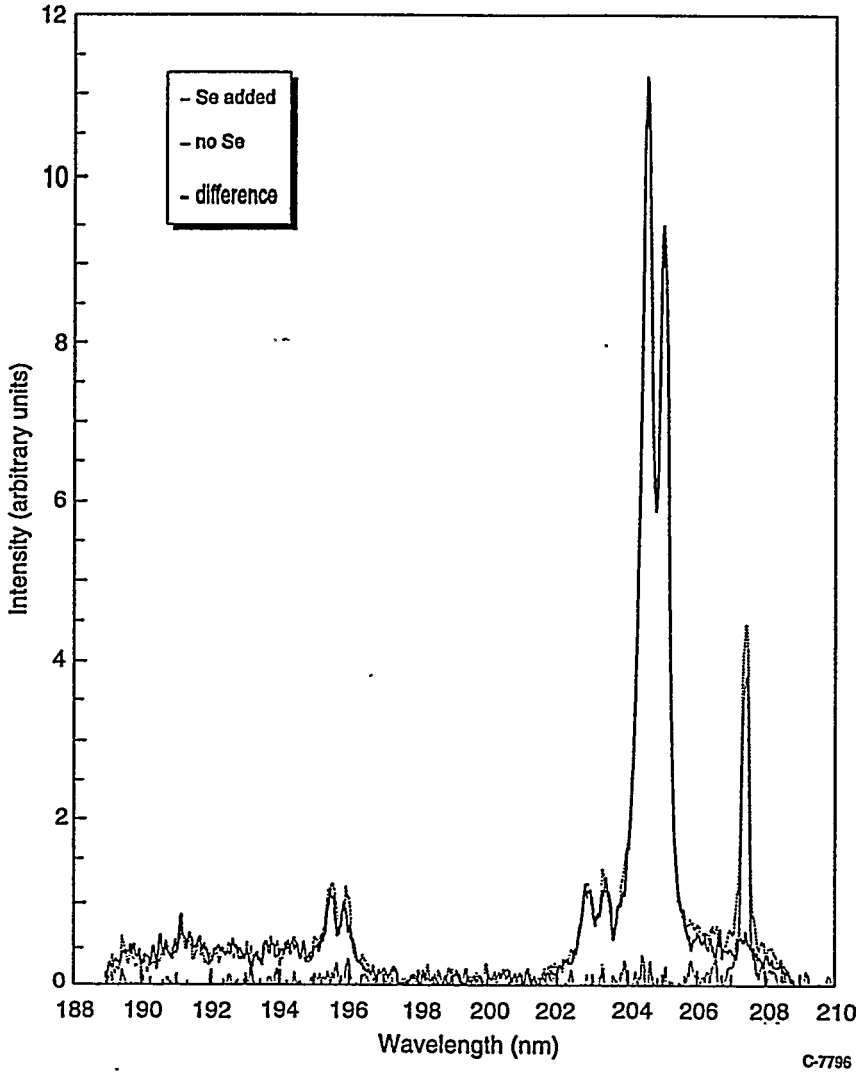

Figure 24. Spectrum between 189 and 209 nm of a dielectric-barrier discharge lamp in nitrogen at atmospheric pressure in the absence of any added Se compound, with 0.024 parts per billion of added Se compound, and the difference between the two spectra.

a few instances we also observed very weak CH($A^2\Delta$ -- $X^2\Pi$) emission at 431 nm. In all cases studied where the organic compound was chlorinated, we observed CCl($A^2\Delta$ -- $X^2\Pi$) emission at 278 nm. We anticipated that we might observe emission from OH($A^2\Sigma^+$ -- $X^2\Pi$) at 308 nm when oxygenated organic compounds were added to the D-B discharge, particularly if alcohols were added. This turned out not to be the case. Presumably the reason for not seeing the OH emission is that it is very efficiently quenched by nitrogen.

Because all species studied behaved similarly, we illustrate our results in the following two sections by considering chloroform, $CHCl_3$ is some detail.

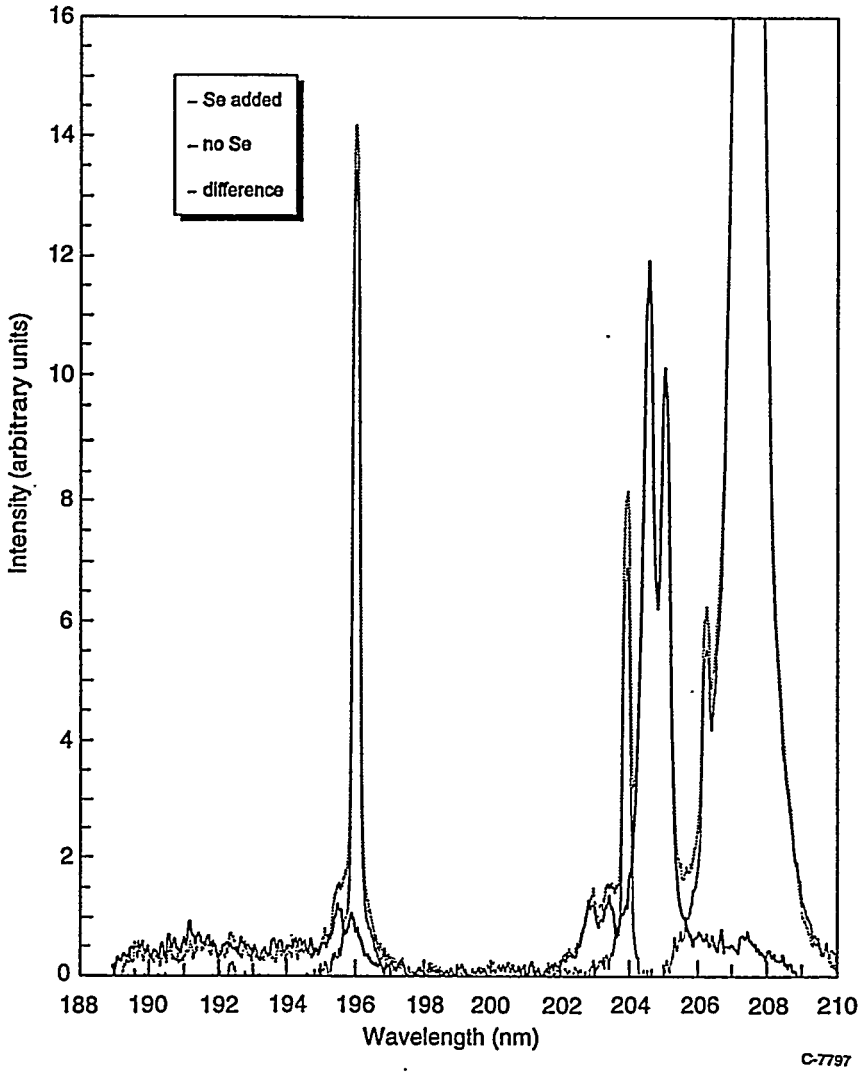

Figure 25. Spectrum between 189 and 209 nm of a dielectric-barrier discharge lamp in nitrogen at atmospheric pressure in the absence of any added Se compound, with 0.50 parts per billion of added Se compound, and the difference between the two spectra.

4.4.1 Detection of Organics

Our results indicate that virtually all hydrocarbons can be detected in a D-B lamp in nitrogen at atmospheric pressure by observing emission from the CN(B - X) system at 388 or 421 nm. Figures 29 and 30 illustrate this at 388 nm. Figure 29 shows the spectra generated in the D-B lamp in the absence of any added chloroform, with 0.05 ppb chloroform added, and the difference between the two spectra, which is a spectrum of just the CN emission. The pure CN spectrum is replotted in Figure 30 for clarity. Figures 31 and 32 show similar data for the region around 420 nm and a chloroform mixing ratio of about 0.01 ppb.

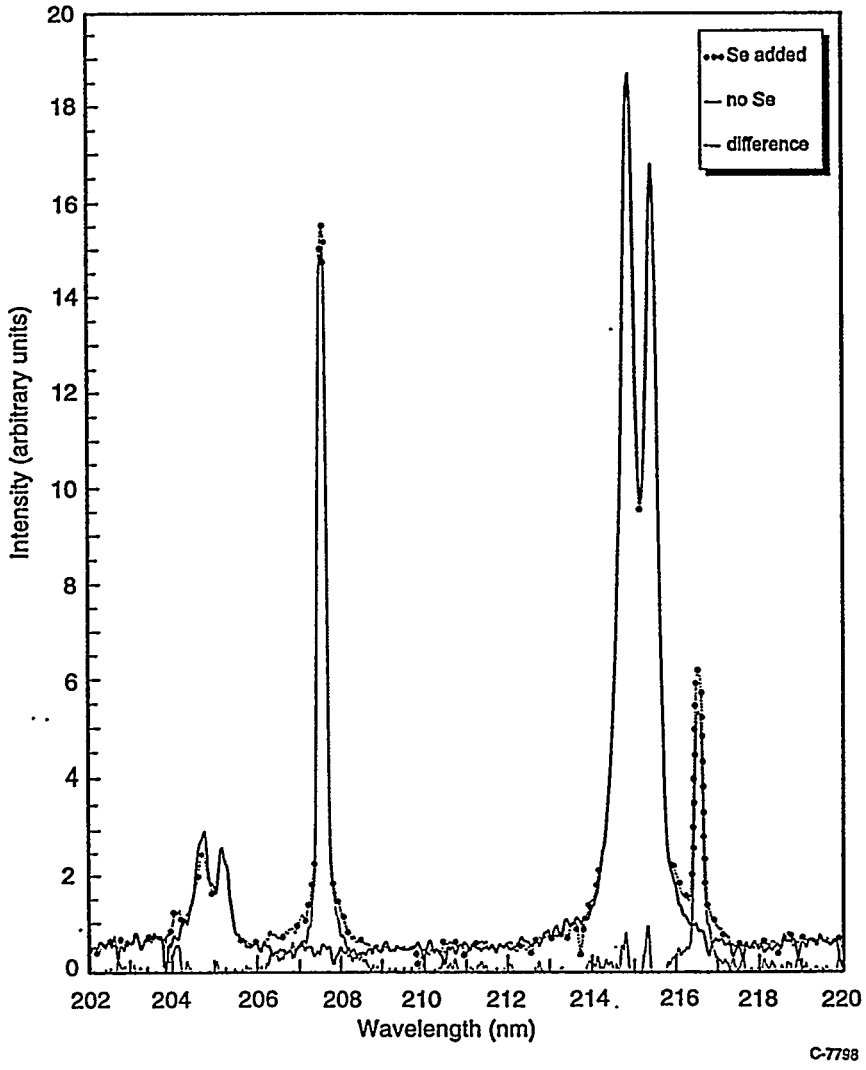

Figure 26. Spectrum between 202 and 220 nm of a dielectric-barrier discharge lamp in nitrogen at atmospheric pressure in the absence of any added Se compound, with 0.036 parts per billion of added Se compound, and the difference between the two spectra.

Figure 33 shows the results of measurements of the integrated intensities of the CN emission as a function of chloroform number density in the D-B lamp. The solid line in Figure 31 is the least-squares best fit to the data. Its slope is 1.3×10^{-6} counts cm^3 molecule^{-1}. Under the conditions of the experiments, a signal of 100 counts would have been readily observable, which would have been produced by having a number density of 7.5×10^7 molecules cm^{-3} of chloroform in the discharge region. Correcting this value for metastable quenching by air means that the minimum detectable number density of chloroform in the sample flow will be about 1.5×10^{11} molecules cm^{-3}. At atmospheric pressure, this number density obtains with a chloroform mole fraction of 7 ppb.

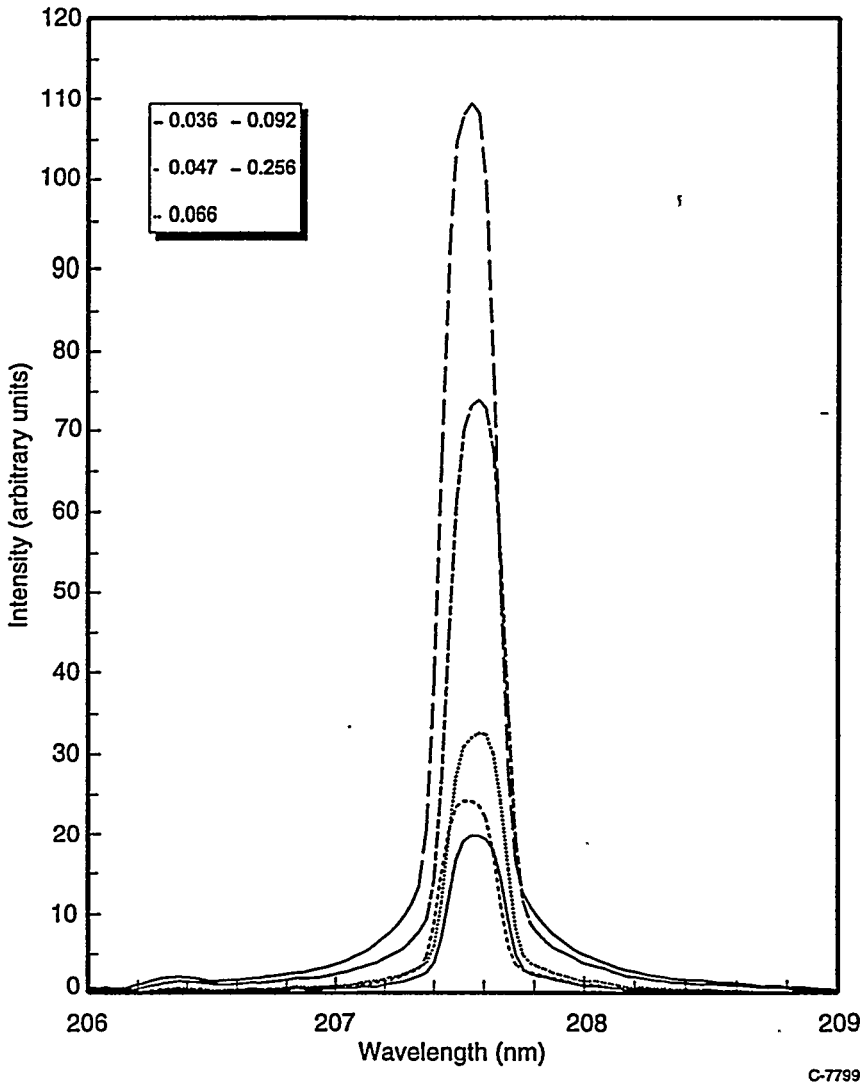

Figure 27. Difference spectra between 206 and 209 nm of D-B discharge lamp in atmospheric pressure nitrogen at five different added mole fractions of a Se compound.

4.4.2 Detection of Chlorinated Organic Compounds

All chlorinated hydrocarbons we have studied manifest CCl emission at 278 nm in addition to the CN emission characteristic of all organic compounds. Figures 34 and 35 illustrate this for the case of chloroform. Figure 34 shows the spectra generated in the D-B lamp in the absence of any added chloroform, with 0.01 ppb chloroform added, and the difference between the two spectra, which is a spectrum of just the CCl emission. The pure CCl spectrum is replotted in Figure 35 for clarity. Figure 36 shows the results of measurements of the integrated intensities of the CCl emission as a function of chloroform number density in the D-B lamp. The solid line in Figure 36 is the least-squares best fit to the data when constrained to give a zero intercept. This slope is 2.2×10^{-6} counts cm^3 $molecule^{-1}$. Under the conditions of the experiments, a signal of 100 counts would have been readily observable, which would have been produced by having a number density of 5.5×10^7 molecules cm^{-3} of chloroform in the discharge region. correcting for metastable quenching by air indicates the minimum detectable signal will be produced by a number

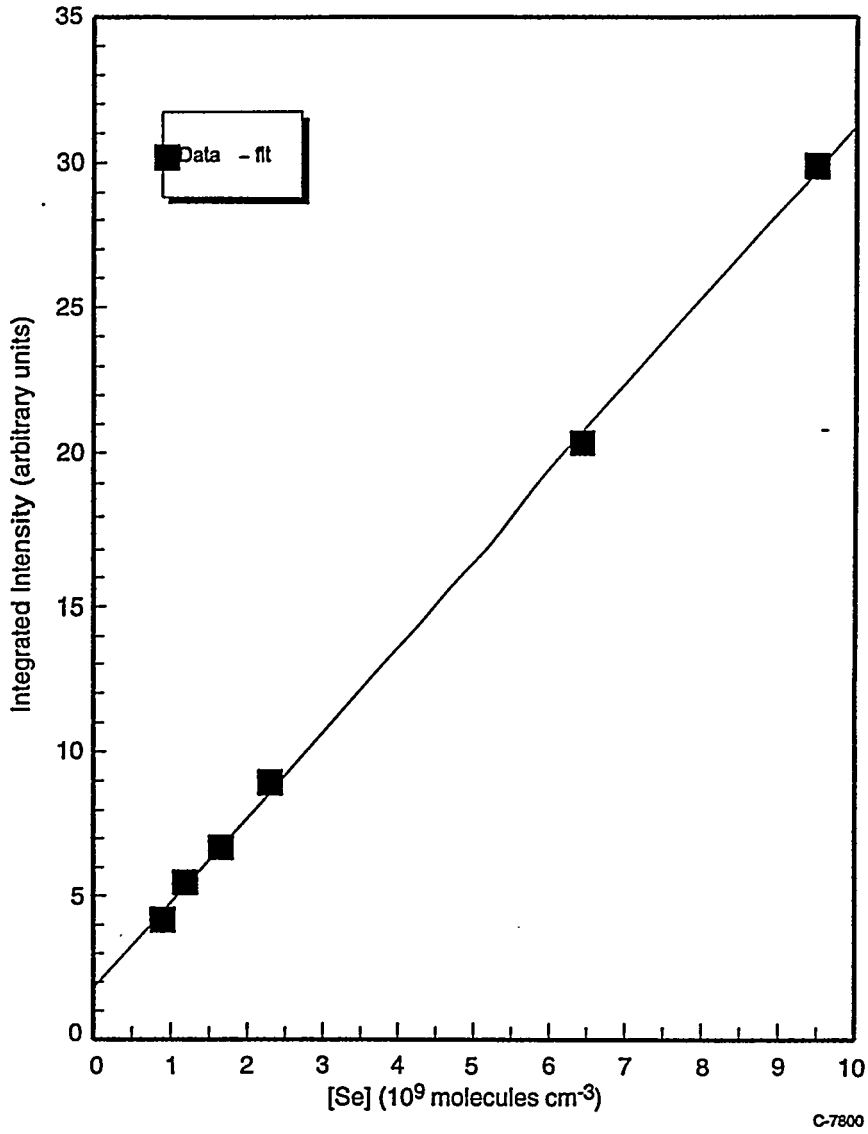

Figure 28. The integrated intensity of the Se line at 207.5 nm as a function of the number density of a Se compound added to an atmospheric pressure N_2 lamp.

density of about 1 x 10^{11} molecules cm^{-3} in the sample flow. At atmospheric pressure, this number density obtains with a chloroform mole fraction of only 4 ppb.

4.5 Experiments with Particulate Samples

In our discussion above on the properties of the microdischarges in the D-B discharge, we suggested that the D-B discharge might be able to detect contaminants on particulates such as fly ash or cement. Ultimately two issues need to be addressed. The first is to determine whether small concentrations of fine dust particles significantly affect the operation of the dielectric-barrier discharge being used in the ANET process. The second is whether hazardous species adsorbed on the dust particles can be vaporized and subsequently detected in the D-B discharge.

We performed a number of experiments where we attempted to entrain particles into a flowing gas stream that then passed through the discharge, or even where we just placed some

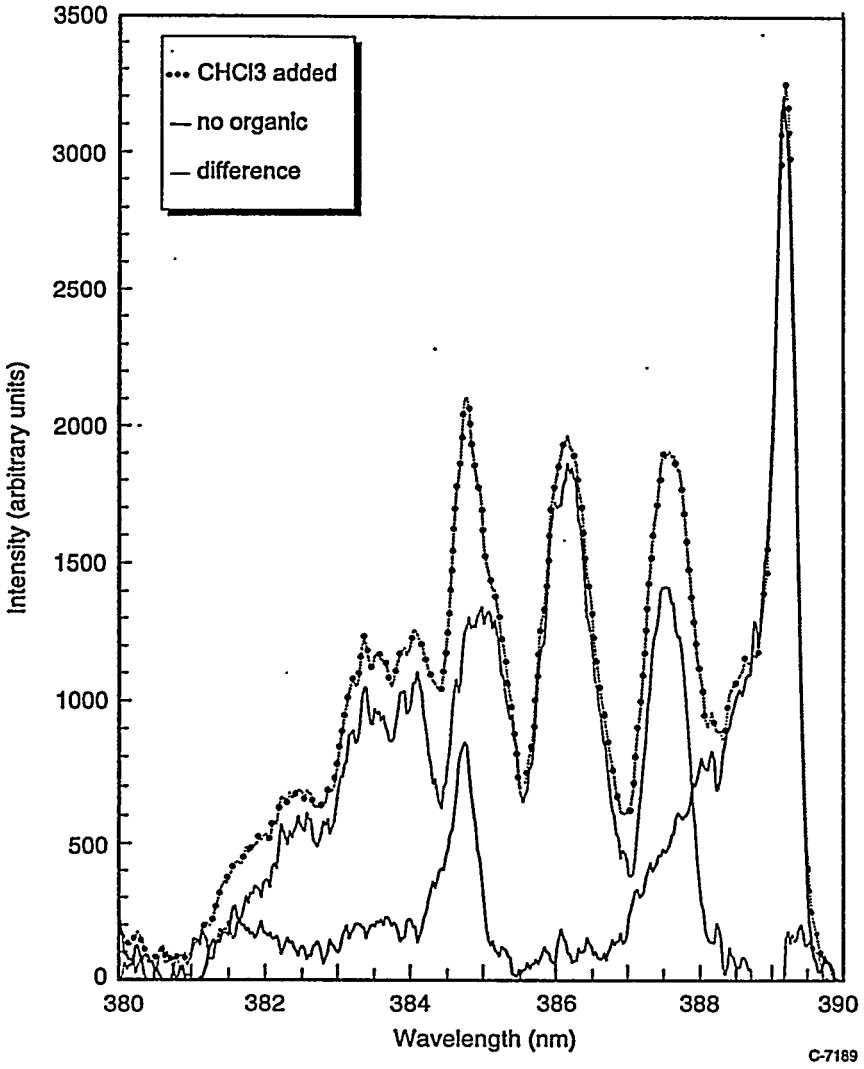

Figure 29. Spectrum around 388 nm of a dielectric-barrier discharge lamp in nitrogen at atmospheric pressure in the absence of any added chloroform, with 0.05 parts per billion of added chloroform, and the difference between the two spectra.

particulate directly in the discharge. Our observations indicated that low particle loadings had a negligible effect on the discharge operation. Very high particle loadings reduced slightly the metastable production in the discharge, but did not seriously compromise metastable production or impair the discharge's ability to operate.

In a second test, we made a simulated cement dust and spiked it by adding a few drops of an aqueous mercury solution, $Hg(NO_3)_2$, to 1 to 2g or dust. The powders used to make the particulate sample were chosen to have the finest possible particle size, generally 10 μm or less. We took spectra of the D-B lamp in the absence of any added dust (or added mercury or any kind), and again after we had placed some of the dust sample in one of the gas lines conducting the nitrogen to the D-B lamp. Figure 37 illustrates the results of that test. The spectrum displayed is the difference between two spectra, one taken before the dust was added to the gas feed line, subtracted from one taken after dust was added to the feed line. The only spectral

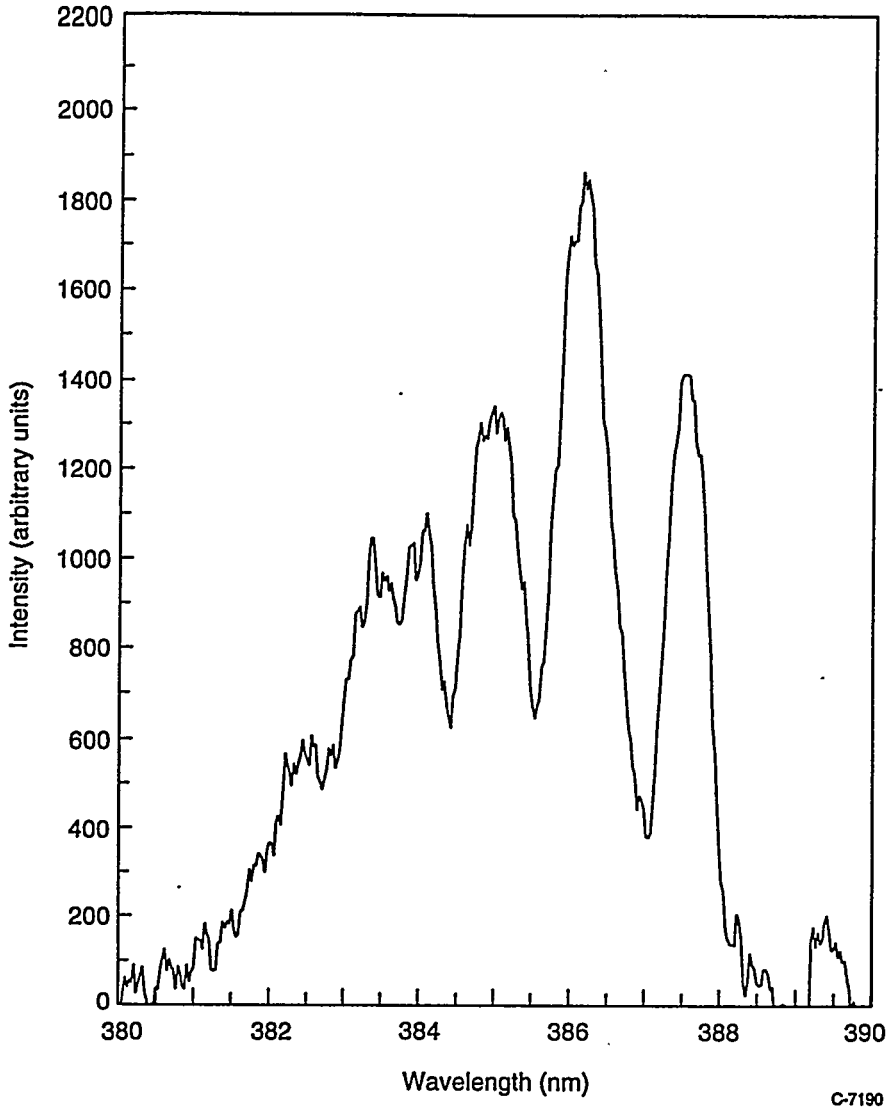

Figure 30. Difference spectrum around 388 nm of D-B discharge lamp in atmospheric pressure nitrogen between the lamp with 0.05 ppb added chloroform and the lamp with no added chloroform.

feature of any significance is the 253.7 nm emission from atomic mercury. This clearly demonstrates that ANET can be used to detect mercury compounds adhering to particulate samples.

4.6 Detection of Uranium Compounds

In a third test, we placed small quantities of a uranium compounds directly in the discharge region. Figure 38 shows the spectrum resulting from the addition of uranyl acetate to the discharge region. Several of the features in the spectrum are easily identified as being part of the nitrogen second-positive system, but three rather broad bands appear at 486, 510, and 534 nm. Figure 39 shows this same spectral region after the second-positive bands and some other background spectral features have been subtracted out. The spectra used to make the subtraction were taken under identical conditions except in a clean lamp from which all traces of the uranium compound had been removed.

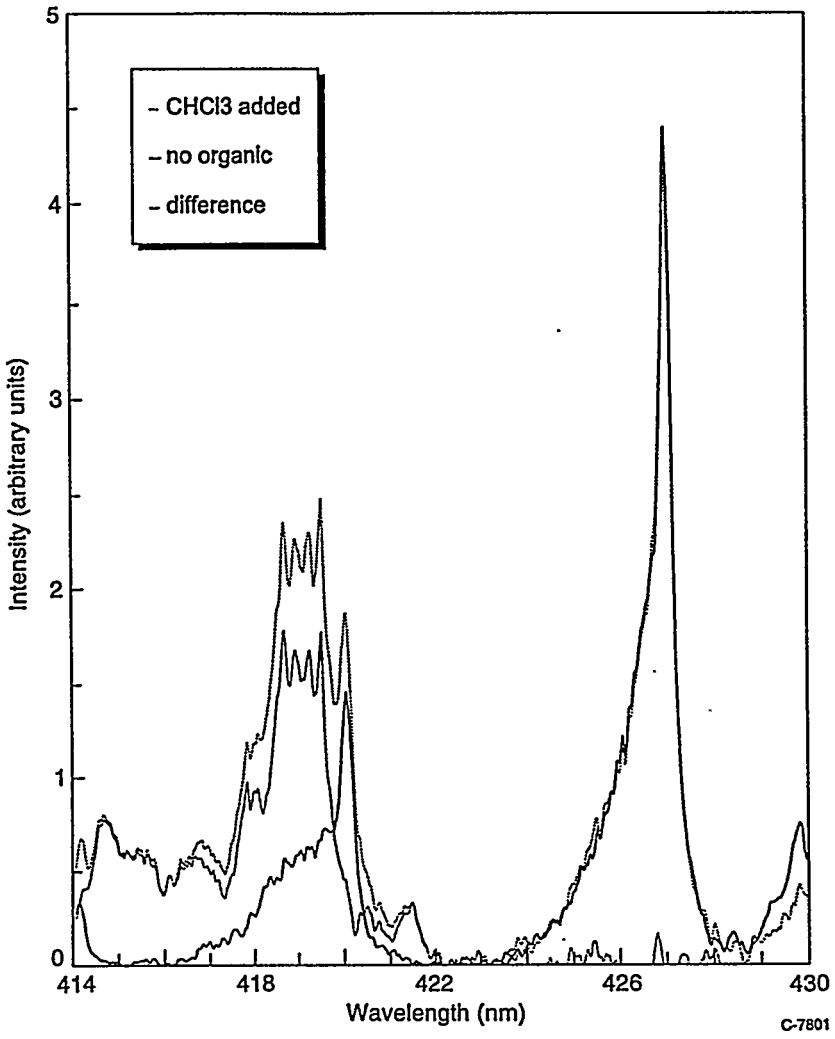

Figure 31. Spectrum around 420 nm of a dielectric-barrier discharge lamp in nitrogen at atmospheric pressure in the absence of any added chloroform, with 0.01 parts per billion of added chloroform, and the difference between the two spectra.

In order to assure ourselves that the observed features were not related to the acetate group in the compound, we repeated the test using uranyl nitrate. The resultant spectrum was very similar. The three bands appeared in the same locations. The only difference is that they appeared to be a little broader when the uranyl nitrate was added.

We think that what we are observing is a spectrum from uranium oxide, probably UO, but possibly UO_2. We surveyed a fairly wide range of wavelengths to see if we could find atomic line emissions from U, but didn't find anything obvious. Since most uranium waste is likely to be oxidized, this probably isn't a serious drawback. We clearly have unique spectral features that identify uranium as being present. Thus ANET appears to have potential for U detection as well as that already demonstrated for other heavy metals.

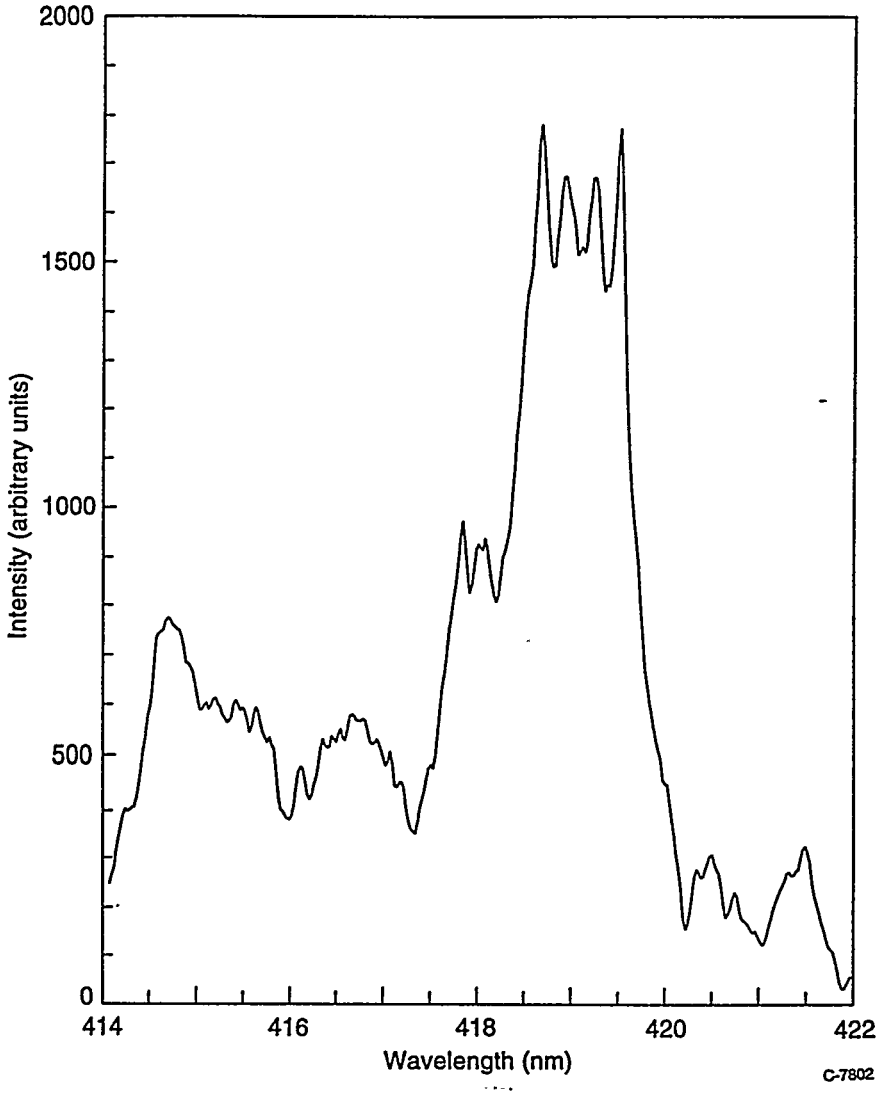

Figure 32. Difference spectrum around 420 nm of D-B discharge lamp in atmospheric pressure nitrogen between the lamp with 0.01 ppb added chloroform and the lamp with no added chloroform.

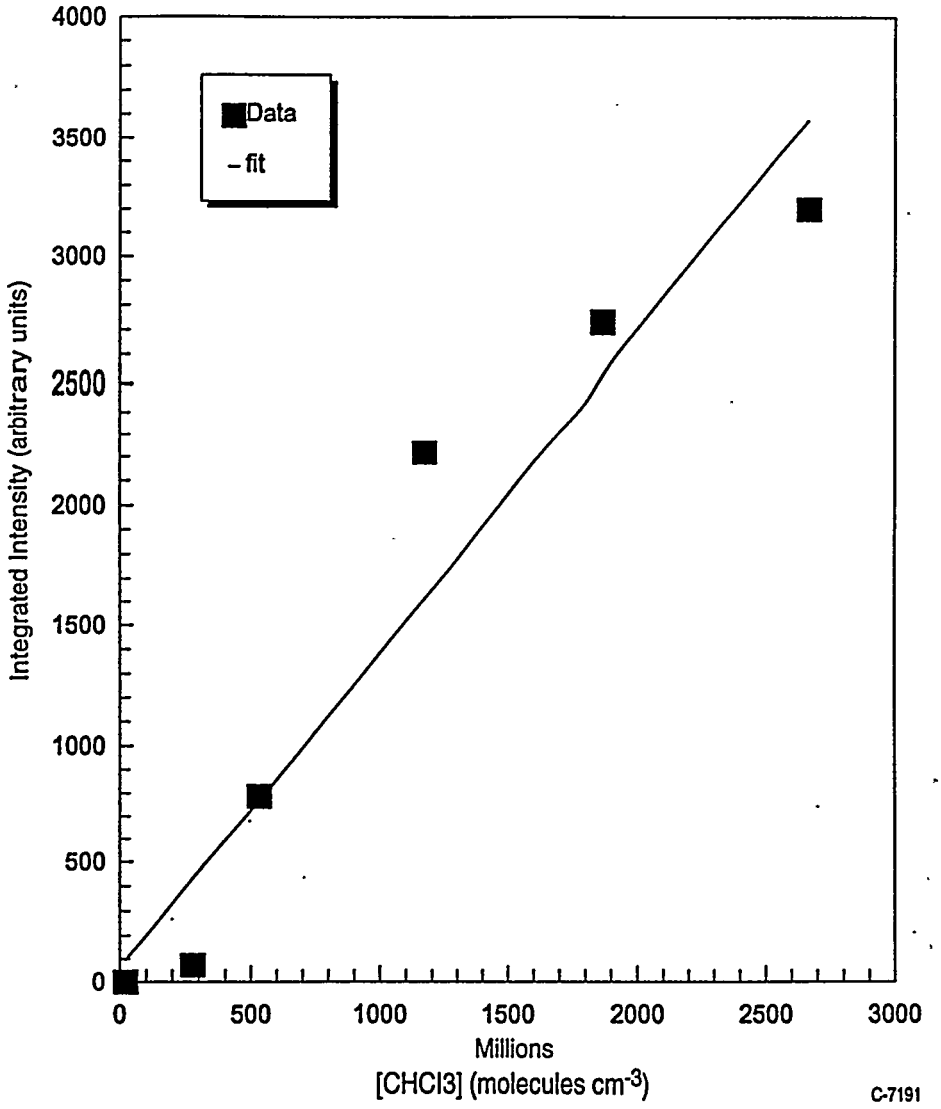

Figure 33. The integrated intensity of the CN band at 388 nm as a function of the number density of chloroform added to the atmospheric pressure N_2 lamp.

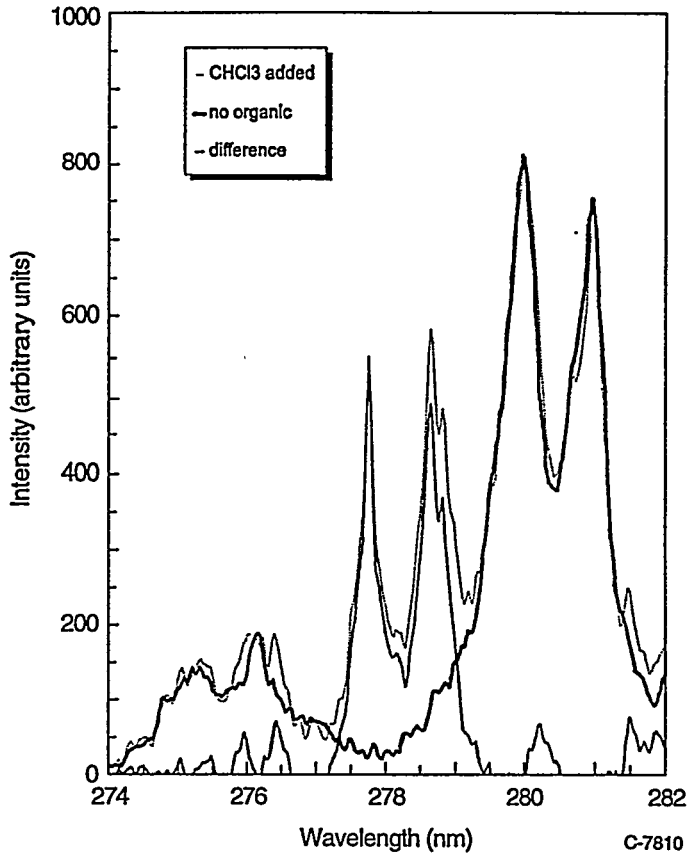

Figure 34. Spectrum of a dielectric-barrier discharge lamp in nitrogen at atmospheric pressure in the absence of any added chloroform, with 0.01 parts per billion of added chloroform, and the difference between the two spectra.

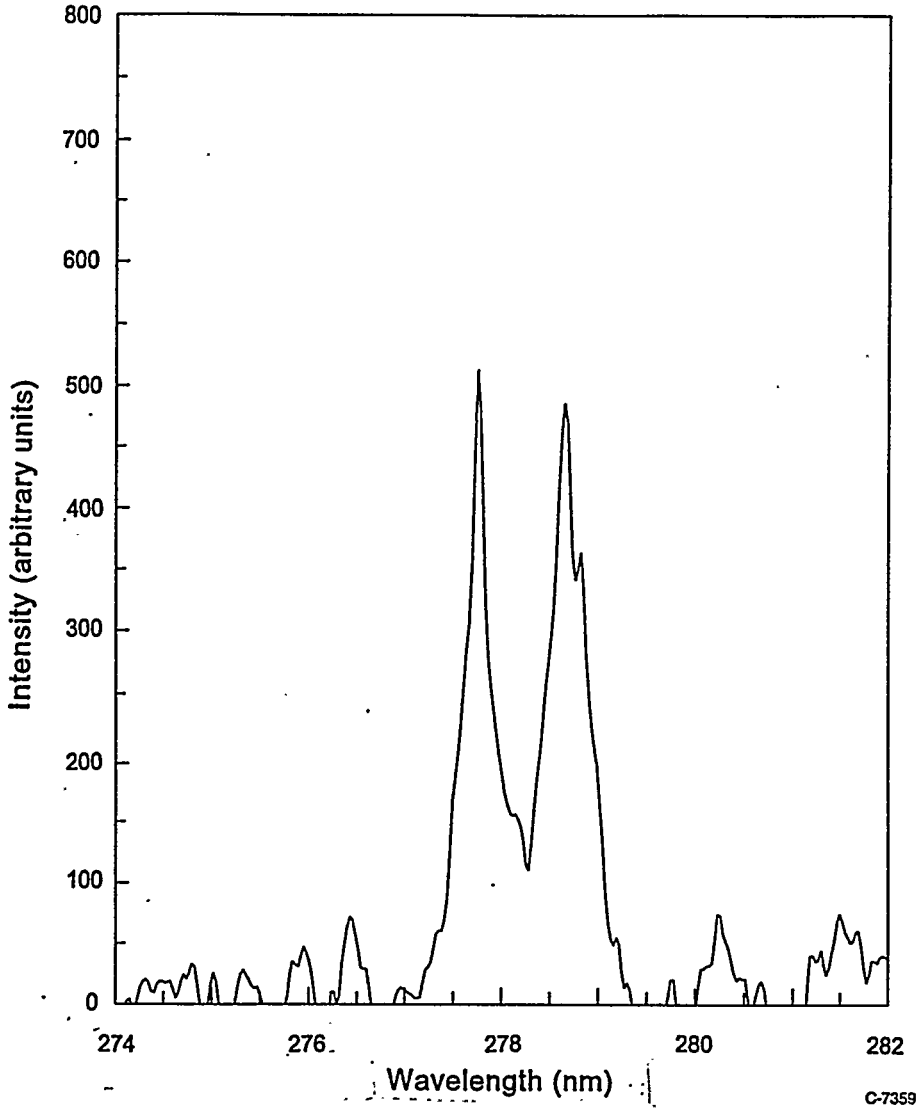

Figure 35. Difference spectrum of D-B discharge lamp in atmospheric pressure nitrogen between the lamp with 0.01 ppb added chloroform and the lamp with no added chloroform.

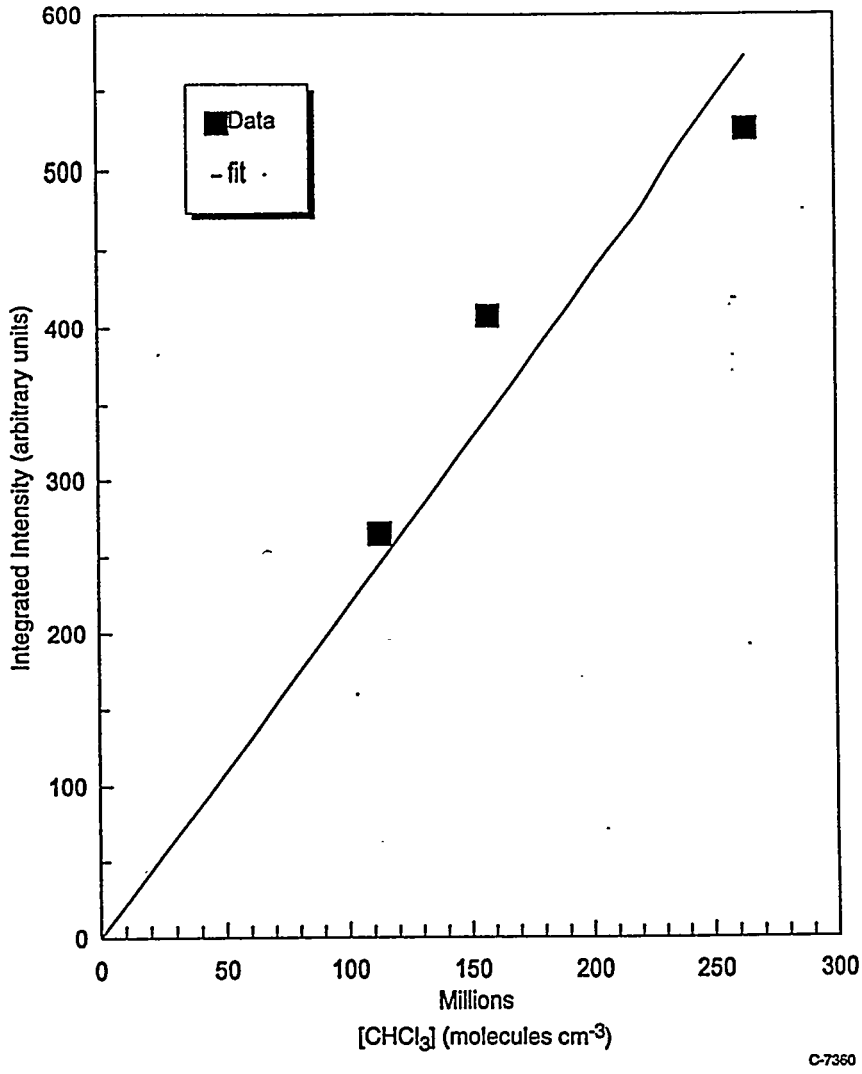

Figure 36. The integrated intensity of the CCl band at 278 nm as a function of the number density of chloroform added to the atmospheric pressure N_2 lamp.

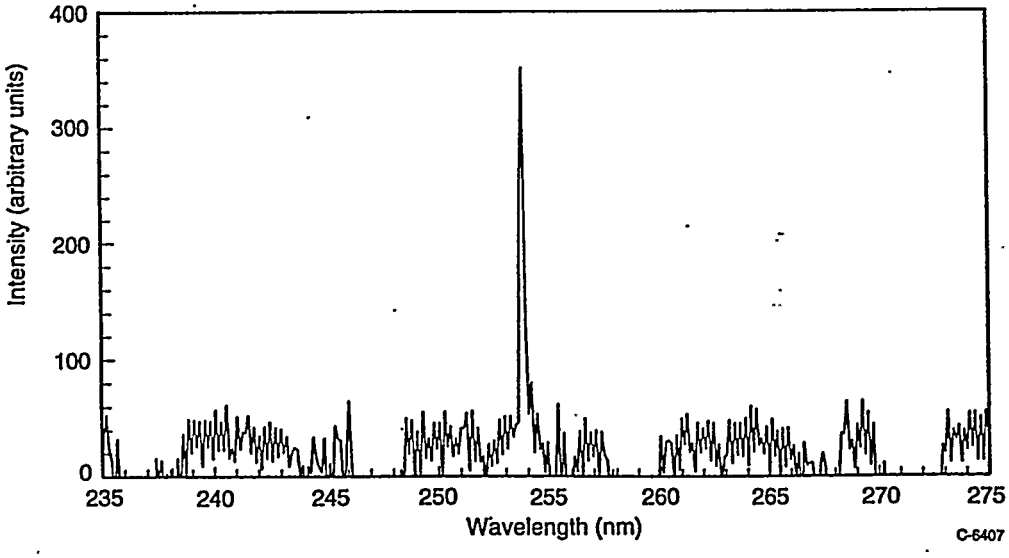

Figure 37. Detection of Hg on spiked particulates.

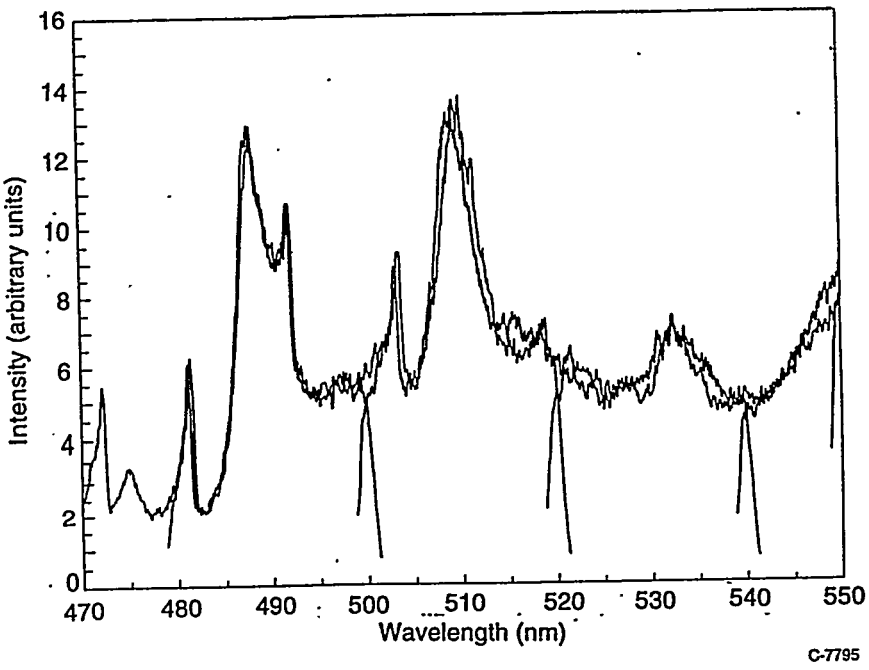

Figure 38. Spectrum of a dielectric-barrier discharge in nitrogen at atmospheric pressure to which a small quantity of uranyl acetate has been added. The spectrum shown is a composite of four separate spectra.

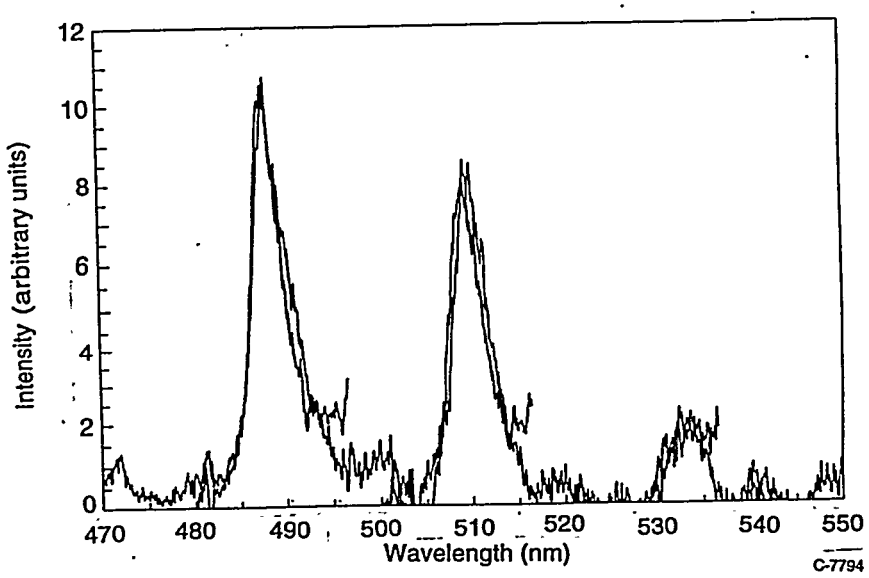

Figure 39. Spectrum of a dielectric-barrier discharge in nitrogen at atmospheric pressure to which a small quantity of acetate has been added. Background spectral features have been subtracted from the spectrum to better display the bands tentatively ascribed to the UO molecule. The spectrum shown is a composite of four separate spectra.

5. PLANS FOR CONTINUED DEVELOPMENT OF ANET

5.1 Introduction

The results of the first phase program successfully demonstrated that the ANET technology holds great promise for development into a sensitive, multi-element hazardous species monitor for use at DOE sites. The goal of the The Phase II effort is to develop and test a breadboard system and use these results to design a prototype field monitor that will be fabricated and tested in the subsequent Phase III program. Early in the Phase II effort we will also conduct a survey of numerous DOE sites to determine the species that are most critical to their needs. This survey will be similar to one that we conducted in Phase I with DOE Headquarters (results described earlier in this proposal). A final objective is to demonstrate the applicability of the ANET technology to additional hazardous species we were unable to address in the Phase I program. The Phase II program objectives are listed below:

Objective 1. Survey several DOE sites in order to identify critical issues for the development of the Hazardous Waste Sensor.

Objective 2. Design, fabricate, and test a breadboard system.

Objective 3. Complete a design for a prototype field instrument

Objective 4. Extend the ANET technology to additional hazardous species.

In order to complete these objectives, we have developed four tasks that are described in detail below. The Phase II program will be very interactive with respect to DOE sites in order to identify critical species and integration issues at the earliest possible time.

5.2 Task 1 - Survey of DOE Sites

In Task 1 we propose to survey numerous DOE facilties to identify critical issues and to establish closer communications with potential end users of the ANET monitor. This coordination will be crucial in the design of the monitor for specific uses at DOE sites.

The survey will be similar to one that we completed with DOE/METC and DOE headquarters during the Phase I effort. The results of that survey indicated that mercury would probably be the most important species at several sites. This provided guidance and helped us tailor the Phase I effort to include mercury as one of the species that we demonstrated in Phase I. The survey will include the following questions.

1. How would you use this monitor? Would it be used during decontamination operations, in site assessment, or in some other operations?

2. What are the likely sample matrices, e.g. water, dirt, blueboard, concrete, etc?

3. What technologies are being used presently and what are their drawbacks? What are your analysis costs (including manpower)? Would your operations benefit from more timely analysis?

4. What are the most important criteria for the new monitor technology (sensitivity, ruggedness, accuracy, reliability, multi-species capability, portability, real-time readout, continuous sampling, speciation)?

5. What are the most important species to be monitored in your facilities? What are the concentration levels?

6. What do you feel are the most important issues for integrating this monitor into your facilities?

Our goal is to gather important information concerning potential sites for the monitor. For those sites that appear to be the best matches for the monitor's capabilities we will conduct site visits to discuss further the integration of the prototype instrument at the end of Phase III. To maximize the coordination with DOE we will invite the DOE COTR to accompany us on these trips. Establishment of these communication lines early in the Phase II effort will help us identify technical issues that can be resolved while the prototype instrument is being designed. For example, we have shown that ANET can detect numerous species and has the potential for monitoring many others. Information on the specific materials to be monitored at a particular site will facilitate the tailoring of the monitor to be most sensitive to those species. This strategy will result in the optimum monitor being delivered to each relevant DOE site.

5.3 Task 2 - Development and Testing of Breadboard Monitor

The primary goals of Task 2 are to develop and test a breadboard instrument. In Task 2 we will establish the procedures for sample handling and analysis and develop systems and software needed to automate these processes. System components asd processes to be examined include sample collection and introduction, active nitrogen stablility, fluorescence detection and analysis, and measurement, calibration, and test procedures.

The primary goals of the second phase of the program are to develop and test a breadboard instrument and to design a prototype instrument suitable for construction and evaluation in the final phase of the program.

The most crucial issues are sampling, calibration, and testing. The other issues, fluorescence detection and analysis, active nitrogen source stability, and measurement procedures, were explored in some detail in the program's first phase. Implementing these components into a breadboard system should be straightforward.

The sampling and testing issues, however, will determine the ultimate success of the ANET technology. Designing a system that abstracts samples truly representative of the hazardous environment is crucial to developing an instrument that can determine hazardous

species concentrations accurately in real-time. Therefore, sample entrainment, speciation, calibration and matrix effects are of primary import.

In order to complete the objectives of Task 2 we have developed several subtasks that we describe in detail below.

5.4 Task 2a - Process Development

As just mentioned above, the purpose of the process development task is to establish procedures for sample handling and analysis, and to develop systems and software to automate these processes. The system and processes to be examined include sample collection and introduction, fluorescence detection and analysis, active nitrogen source stability, and measurement, calibration, and test procedures. The crucial issues are sampling, calibration and testing. It is critical that we design the sampling system to accurately measure the true hazardous species concentrations in a realistic environment. Therefore, sample entrainment, speciation, calibration and matrix effects become important. These issues are discussed below as they impact the specific system component or process.

The sampling and testing issues will ultimately determine the degree of success of this technology. The other issues, fluorescence detection and analysis, active nitrogen source stability, and measurement, either contain less risk or already have clearly identified and satisfactory solutions from the results of the first phase.

5.4.1 Sample Introduction

The simplest form of sampling would involve particle introduction by entraining dust particles from the building material to be tested into a flow of nitrogen and then injecting this sample directly into the dielectric-barrier discharge region. Ideally the sample will be drawn into the instrument through a flexible hose that can be maneuvered easily to the sampling location of interest. Although dust could be removed directly from the surface in this manner, a better sampling procedure might be to dislodge some of the dust from the surface to be tested into the surrounding air, and then extract a sample of the airborne particles. An advantage to this technique is that one could delay sampling briefly to allow larger particles to settle out of the sample volume. Smaller particles will be more readily vaporized in the discharge. In addition the smaller particles are likely to have greater concentrations of the toxic species which will allow more sensitive analyses.

We will determine how best to dislodge particles from surfaces for analysis so that analyses can be performed in a consistent, uniform manner. The surface could be subjected to a puff of air or to a small impact of some sort. It will be important to have the air puff or impact be of consistent strength each time. This can be easily done using a pulsed valve and appropriately designed nozzle to release air puffs. Mechanical shock can be supplied uniformly using a spring driven impactor of some sort (at PSI we have extensive experience with small impactors of this kind). Some combination of these two ideas might be necessary. Initially flooding the surface to be tested with nitrogen will minimize the amount of oxygen entering the discharge with the

sample. This will then help maintain high metastable number densities within the discharge and reduce impurity emissions.

Alternative sampling procedures may need to be investigated including surface scraping and chemical pretreatment. This latter approach reduces the simplicity of our analytical technique and will be avoided if at all possible. It is important, however, to be prepared for all eventualities. It may prove necessary to determine particle loadings in each sample. This can be done in straightforward fashion using battery-powered, miniature diode lasers for particle extinction and scattering measurements. We are very experienced in such techniques.

The advantage to this direct sampling procedure is a lack of preference for any specific molecular form of a hazardous material. The distribution of the toxic species among their various molecular forms is preserved. Other possible forms of sample introduction that include heating or another form of energy deposition may speciate the compounds and produce non-representative results. We will not use such methods. This issue is related to testing and calibration, as presented later.

5.4.2 Fluorescence Detection and Analysis

Our proposed technique for fluorescence detection is to using a small spectrograph to disperse the radiation and an optical multichannel analyzer (OMA) to detect it. Such a detection system gives a complete spectrum of the spectral region covered by the OMA. Because of this feature, fluorescent emissions from a host of different species can be detected simultaneously. Given the multi-element capacity we are designing for, the OMA is still our first preference. However, we will also investigate the possibility of employing a limited set of optical filters with a simple detector. The advantages of the filter approach are reductions in cost, size, and power. The principal disadvantage is a reduction in the number of detectable species. We will perform a cost/benefit analysis for these two alternatives.

The OMA system we have used most widely at PSI consists of a 0.32m focal length Instruments SA spectrograph and a Princeton Instruments Inc. Model 110 OMA. The OMA consists of a reticon array containing 1024 elements, 750 of which are intensified, each 0.025 mm wide. The OMA has an extended S-20 response (200 to 900 nm), with a quantum efficiency of about 20% in the visible. The read-out time of the OMA, or the minimum time for acquisition of a complete spectrum, is 16.2 ms (60 Hz). The OMA software allows the instrument to average a number of sequential spectra to improve signal-to-noise in the detected signal.

The extent and resolution of each spectrum is determined by the dispersion of the grating in the spectrograph and by the width of the OMA pixels. With a 600 l mm^{-1} grating in the 0.32m spectrograph, the reticon array would cover approximately 150 nm and provide a minimum resolution of about 0.6 nm (using 5 pixels as the definition of instrument resolution).

We will determine the best balance between spectral coverage and instrument resolution. Increasing the resolution, by using a grating of higher dispersion, will reduce overlap between adjacent lines. This will give a more precise determination of atomic fluorescence intensities. The

drawback to high resolution is that signal levels are smaller and the OMA covers narrower spectral range. Increasing the spectral range reduces resolution which may lead to larger uncertainties in determining fluorescence intensities of closely spaced species. On the other hand, the greater spectral coverage may allow additional species to be detected simultaneously or provide additional lines for analysis of a given species, thereby reducing the effects of spectral overlap. Our prior experience indicates that a spectral resolution at least as large as 0.4 nm is adequate to ensure good separation of neighboring lines. In this program we will determine if a somewhat larger resolution will still be sufficient.

The design choice of spectral coverage is driven by the fact that some emissions important for identifying and quantifying certain species may be outside the range covered by the spectrograph. In this case the spectrograph grating could be stepped to allow coverage of another spectral region. Rotating the grating will permit measurements in the new wavelength region in less than a second. Spectra in this new wavelength region could be taken with little change in conditions from the initial spectral region. We will attempt to minimize or avoid grating movement if possible. An additional possibility would be to set the grating to cover an appropriate spectral region in the visible, and to observe ultraviolet features in second order. Then all that would be needed would be order sorting filters that could be slid across the spectrograph's entrance slit using a solenoid.

A major advantage of ANET is that the generated fluorescence occurs on only a few characteristic emissions, the intensity of each is fixed ratio to others. Even if several strong emissions from a particular atom or radical are overlapped by emission features of other species, the species interfering at one wavelength will be different from those interfering at another wavelength. The concentrations of the various contaminants can be determined, therefore, using a pattern recognition procedure similar to those used to identify compounds from mass spectral cracking patterns.

An additional potential source of spectral interference is the naturally occurring emission in a nitrogen D-B lamp. We demonstrated in the phase I program that this background emission is readily characterized and can easily be subtracted from observed spectra to obtain clean spectra of the additive species. We will exploit this feature of the system in our analysis routines.

5.4.3 Active Nitrogen Source and Stability

We have shown in the first phase of this program that the intensity of the fluorescence excitation, and thereby the sensitivity of the proposed analytical technique, is proportional to the metastable nitrogen number density in the discharge region. Thus, to ensure uniform excitation conditions from one sample to the next, it may be important to have a technique to monitor the metastable number density. Initial testing may show that metastable number densities in the discharge are invariant from sample to sample and over time. In that case, a metastable monitor would not be necessary in the final instrument. In initial development stages, however, one should be able to monitor the metastable number density in the discharge.

Our experience on the first phase has shown that a direct measurement of the Herman infrared emission is the best way to monitor the metastable number density. The intensity of the Herman infrared emission is directly proportional to the square of the metastable $N_2(A)$ number density. Testing of our system in this phase with various samples and under various conditions will indicate whether such a diagnostic is necessary. If this proves to be the case then we will construct a Hermen infrared diagnostic from a narrow bandpass filter and a photodetector.

5.4.4 Measurement Procedures

The measurement procedures will be automated so that operator intervention will be minimized. We anticipate that samples will be entrained directly from the building materials or other sample matrices into the discharge region where fluorescence excitation and detection will occur under computer control. We also plan to automate data analysis and the identification and quantitation of species present in the sample. The primary requirement for operator intervention, therefore, will be in the actual collection of the samples. We will design a system where the operator will position the sampling tube over the surface to be tested and then activate the sample collection system. The rest of the sample collection and analysis will proceed under computer control. The goal of this task will be to develop these automated procedures. We will make extensive use of graphical user interface (GUI) methods.

5.4.5 Calibration and Test Procedures

Calibration and testing are key to the success of this technology. The reason is that the monitor must be developed to accurately detect species as they are expected to occur at DOE sites. This refers to their likely sample matrices, concentration ranges, and distribution among their various chemical forms. If we we test and calibrate accordingly, the instrument that results will accurately measure the hazardous species, thereby avoiding downtime, program delays, and incurred costs.

An example of this issue is mercury speciation. In addition to the elemental form, mercury can exist as the chloride, oxide, and in various organic forms. A detector developed to measure only one of these will fail at a site dominated by the other forms. It is therefore crucial that we design our instrument knowing as much of actual requirements or anticipated requirements as possible. As part of this task, therefore, we propose to resolve the detector requirements in discussions with DOE representatives. This will include the full complement of species desired, their speciation, and the known or anticipated sample matrices. These discussions will not preclude later extension of this technology to other species of interest. Our design will be performed such that such upgrades will be possible.

Initial testing and calibration will use samples we purchase from environmental standards supply houses or we prepare ourselves. We will also consult with DOE engineers. We will use several standards for each element, each having different contaminant concentrations. By comparing different samples of the same element, we can demonstrate our technique is not compromised by dilution effects. These tests will also show if emissions from several contaminants overlap with each other. Such interferences are not likely to cause problems with our

technique for two reasons. First of all, ANET results in only a small number of fluorescencelines or bands from each contaminant species. Thus, separating emission lines from the different elements should not be particularly difficult. Second, our technique allows simultaneous measurement of all emission lines from any given species. As a result, any interference from a particular emitter at one wavelength should be absent at other wavelengths characteristic of the species being detected. In addition, our pattern recognition procedure generally cancels any interferences that might obtain in multi-element samples.

Freedom from the interfering fluorescence from other emitters is, as we have mentioned above, not only a function of the number of emission lines from the various elements, but also a function of the resolution of the spectrograph. Our initial series of calibration runs will focus on determining the spectral resolution that balances the freedom from interference from neighboring fluorescence lines with signal levels giving adequate sensitivity to detect metal contaminants at levels below which they pose no threat to the environment.

Finally our experiments will explore the issues of sample-to-sample independence and whether or not the sampling procedures we employ affect the stability of the active nitrogen source. It is absolutely crucial that the results from the analysis of a given sample are in no way compromised by the samples that preceded it. A number of analyses to be run successively, without special probe cleaning precautions in between, will assure ourselves of sample independence.

The results of these experiments are essential for determining the best methods of sample handling, data collection, and data reduction. The design of the sample inlet and the necessary spectral resolution and range will all be dictated by the results of these experiments. In addition, all of the important characteristics of the analytical technique will be determined. These characteristics include ultimate sensitivity, freedom from interference with multi-element samples, freedom from matrix effects, sample-to-sample independence, and source stability.

5.4.6 Task 2b - Process Integration

We will integrate the procedures developed in the tasks outlined above into a standardized measurement protocol. This will allow us to determine which steps can be fully automated and which ones require operator intervention. In addition, software for apparatus operation, data collection, and data analysis will be developed under this task.

The analytical procedures used to collect the data under this task will be developed carefully so that they can be broken down into a series of individual steps. Techniques for implementing each step will then be tested to ensure that doing them in a carefully prescribed fashion will give reproducible results. Computer software will be developed to control those steps that lend themselves to automation. We have considerable experience in these methods. These steps will include setting gas flows and collecting and storing fluorescence spectra.

Steps requiring operator intervention also will be broken down so that they are accessible to operators with relatively limited technical background and experience. We will write simple,

step-by-step instructions for the analysis. As much as possible, we shall try to incorporate the steps into the instrument design so that each step can be cued in a logical order. Some of this cuing might appear on the screen of the system's computer while other cuing would be built into the instrument itself using appropriately numbered or colored buttons. The above process will create an operation "procedure" for performing analyses with the prototype instrument to be fabricated under the final phase.

Where possible, we shall incorporate commercially available software into the apparatus. Software is very time consuming and expensive to develop, so incorporating software that has already been developed and tested will result inconsiderable savings both in time as well as in money. Some of the major software needs will be to control processes such as gas flow rates and discharge current, to collect experimental data such as reactor pressure, and intensity of the active nitrogen monitor (if needed), to record the atomic fluorescence spectra, and to analyze the data.

This last step will involve identifying the fluorescing species and relating their intensities to concentrations. Determining species concentrations will involve integrating the fluorescence from each of the different elements over the analysis time, normalizing these integrated intensities by the intensity of the active nitrogen monitor, and then relating the normalized intensities to concentrations using a set of calibration factors determined from runs on known standards.

The analysis steps are quite similar to those used in other analytical techniques. The identification of a characteristic spectrum of a given element composed of fluorescence from lines at several different wavelengths, each having a fixed intensity in relation to the others, is very like the identification of complex molecules in mass spectrometric analysis based upon characteristic cracking patterns. Instruments based upon mass spectrometric detection generally contain a library of fragmentation patterns. Our work in this task will determine the intensity distribution of the characteristic fluorescence lines from each species and these distributions will be used to develop our "standard" patterns.

We already have an extensive background in using computers to collect data or to control devices. Most of our work also involves the use of commercially available software, so adapting our current processes to the anticipated needs of this program should be relatively straight forward. For example we have developed several diode laser based gas monitors that are computer controlled. Interfacing is by simple GUI windows.

5.4.7 Success Criteria and Deliverables

The success criteria for the Process Development task are more challenging and detailed than those of the first phase. They are:

- Demonstrate an efficient, non-destructive sample introduction method;
- Demonstrate an analysis protocol that results in consistent, reproducible results for test species under simulated "real" conditions;
- Demonstrate the analytical technique is free from interference between elements.

The principal deliverable for this phase (task) will also be a report. The report will summarize the work performed towards the development of this technology as a true analytical method. Demonstration of adequate sensitivity to most of the target compounds under calibration and simulated "real" conditions is key. A critical component of this is the sample introduction method. We are proposing a non-destructive sample introduction method as such a passive technique will encounter the fewest compliance problems. Other possible techniques, including sparks and laser ablation, involve localized surface energy deposition that will be a possible ignition source. We will, however, investigate other passive alternatives. The report will also include a discussion of the proposed integrated system, complete with capabilities and shortcomings. These will be contrasted with DOE needs to determine whether the technology warrants further development. A sponsor briefing to discuss these issues in person will be included at the completion of this task.

5.5 Task 3 - Design Engineering

5.5.1 Design Engineering Activities

The design engineering task has two elements. The first of these is to identify and specify each of the components to be incorporated into the prototype instrument we shall fabricate as a part of the final phase of the program. Each component needed will be enumerated, and commercial suppliers will be identified. We will investigate the efficacy of in-house construction of some components versus their purchase from commercial OEM suppliers. Final component suppliers will be determined by balancing various factors, including adaptability, quality, size, weight, and cost.

The second element of the design engineering task is to design a prototype hazardous waste monitor. This design will balance a number of considerations including power management and portability. The location of each component will be studied in relation to the others to identify configurations that promote simple operation and servicing while retaining compactness in the whole instrument. At the end of the program's second phase we will have a detailed set of drawings and specifications for the construction of a first-generation, or alpha-, prototype instrument.

The purpose of the design engineering task will be to identify and specify each of the components to be incorporated into the prototype instrument we shall fabricate as a part of the program's final phase. Each necessary component will be enumerated, and commercial suppliers will be identified. We will investigate the efficacy of in-house construction of some components versus their purchase from commercial OEM suppliers. For example, Princeton Instruments, the manufacturer of the OMA, has already indicated that they would supply OEM models at significant cost savings. The final component suppliers will be determined by balancing various factors, including adaptability, quality, size, weight, and cost.

A second component of this task will be the design of a prototype hazardous waste monitor. This design will balance a number of considerations including power management and portability. We will use an ALGOR computer-aided design system (CAD) to aid the design.

Among other uses, we have relied heavily on it during the design of several of our space instrument packages. The location of each component in relation to the others will be studied to identify configurations that promote simple operation and servicing while retaining compactness in the whole instrument.

We will also interact heavily with our subsidiary company PSI Environmental Instruments Corporation. They were spun off recently to commercialize several instruments developed under successful SBIR programs. They have recently begun delivering instruments to the power generation industry to monitor and control combustor temperatures and to measure concentrations of ammonia in gas streams. They have extensive experience and capabilities in system engineering and field testing of instrumentation in hostile environments.

5.5.2 Design Engineering Success Criteria and Deliverables

The success criteria for this task are as follows:

- Production of engineering drawings and technical specifications for the manufacture of a prototype instrument;
- Development of a cost estimate for instrument manufacture;
- Successful integration of component package into size, weight, and power specifications suitable for portable, field-operable instrument;
- Development of a commercialization plan for the ANET technology.

This phase will also conclude with a report and a sponsor briefing. In contrast to the previous tasks, however, the emphasis will be on economic and commercialization issues. The results of the engineering study will be reported. Based on this, an accurate assessment of the system cost will be determined. We will include in the report an updated and accurate costing for the final phase. A preliminary version was submitted with the original proposal. These preliminary data will be updated in light of the results of the preceding research, the determined system cost, and through discussions with the sponsor. To complete the economic evaluation, we will include a commercialization plan for this technology in the report for this task. Finally, we will deliver a complete set of engineering drawings and component specifications to the sponsor.

5.6 Task 4 - Diagnostic Extension

Activities on this task will follow procedures developed during the first phase of the program. The main purpose of this task will be to establish sensitivities for detecting additional hazardous species of interest to the sponsor that were not addressed in the first phase of the program. The list of species will be determined in consultation with the sponsor's needs. Likely candidate species would include heavy metal products from nuclear fission such as Cs and Sr, and other toxic heavy metals such as Cd and As that are somewhat more difficult to detect sensitively by more conventional means. Since we have discussed our apparatus and procedures in detail

above, and since these proposed investigations will be similar to those already done, we will not discuss them further here. Suffice it to say we wish to be responsive to the needs of DOE and will make every effort to address the toxic species of greatest importance to it. This task will allow some extension to other species that could be included in later designs of fielded monitors.

REFERENCES

1. Perkin-Elmer Corp., "A Guide to Techniques and Applications of Atomic Spectroscopy", Norwalk, CT (Perkin-Elmer Corp.) (1988).

2. Wright, A.N., and Winkler, C.A., Active Nitrogen, New York: Academic Press (1968).

3. Capelle, G.A. and Sutton, D.G., "Analytical Photon Catalysis: Measurement of Gas Phase Concentrations to $10^4/cm^3$, " Appl. Phys. Lett. 30, 407 (1977).

4. Wittman, P.K., and Mitchell, J.W., "Ultrapurification of Nitrogen Monitored by Metastable Transfer Emission Spectroscopy," Appl. Spectrosc. 40, 156 (1986).

5. Capelle, G.A. and Sutton, D.G., "Metastable Transfer Emission Spectroscopy--Method and Instrument for Detection and Measurement of Trace Materials in Gas Flows," Rev. Sci. Instrum. 49, 1124 (1978).

6. Jurgensen, H. and Winefordner, J.D., "Use of Active Nitrogen in Analytical Chemi-luminescence Spectrometry," Talanta 31, 777 (1984).

7. Neimczyk, T.M. and Na, H.C., "Metastable Transfer Emission Spectroscopy," Appl. Spectrosc. Revs. 19, 363 (1983).

8. Golde, M.G., "Reactions of $N_2(A^3\Sigma_u^+)$, Int. J. Chem. Kinet. 20, 75-92 (1988).

9. Piper, L.G., Kessler, W.J., Fraser, M.E., and Davis, S.J., "Quantitative Lubricating Oil Debris Monitoring and Analysis," Final Report prepared for Naval Sea Systems Command, PSI-11-1/TR-1095, January, 199 1.

10. Eliasson, B. and Kogelschatz, U., "UV Excimer Radiation from Dielectric-Barrier Discharges", Appl. Phys. B 46, 299(1988).

11. Eliasson, B. and Kogelschatz, U., "The Silent Discharge and its Application to Ozone and Excimer Formation", in Nonequilibrium Processes in Partially Ionized Gases, M.Capitelli and J. N. Bardsley eds., New York: Plenum Press, pp. 401-410 (1990).

12. Kogelschatz, U., "Silent Discharges for the Generation of Ultraviolet and Vacuum Ultraviolet Excimer Radiation", Pure & Appl. Chem. 62, 1667 (1990).

13. Braun, E., Kiichler, U., and Pietsch, G., "Microdischarges in Air-fed Ozonizers", J. Phys. D.: Appl. Phys. 24, 564 (1991).

14. D'Silva, A.P., Rice, G.W., and Fassel, V.A., "Atmospheric Pressure Active Nitrogen (APAN)-A New Source for Analytical Spectroscopy", Appl. Spectrosc. 34, 578 (1980).

15. Rice, G.W., D'Silva, A.P., and Fassel, V.A.,"Analytically Useful Spectra Excited in an Atmospheric Pressure Active Nitrogen Afterglow", Appl. Spectrosc. 38, 149 (1984).

16. Wulf, O.R. and Melvin, E.H., "Band Spectra in Nitrogen at Atmospheric Pressure. A Source of Band Spectra Excitation", Phys. Rev. 55, 687 (1939).

17. Cummings, W.P. and Piper, L.G., "Production of $N_2(A^3\Sigma_u^+)$ in the Low pressure Dielectric-Barrier (Ozonizer) Discharge", Appl. Spectrosc. 44, 656 (1990).

18. Piper, L.G., "Reevaluation of the Transition-Moment function and Einstein Coefficients for the $N_2(A^3\Sigma_u^+ - X^1\Sigma_g^+)$ Transition," J. Chem. Phys. 99, 3174 (1993).

19. Dreyer, J.W., and Perner, D., "Deactivation of $N_2(A^3\Sigma_u^+, v=0\text{-}7)$ by Ground State Nitrogen, Ethane, and Ethylene measured by Kinetic Absorption Spectroscopy," J. Chem. Phys. 58, 1195 (1973).

20. Piper, L.G., Caledonia, G.E., and Kennealy, J.P., "Rate Constants for Deactivation of $N_2(A)$ v'=0, I by 0_2, " J. Chem. Phys. 74, 2888 (1981).

21. Piper, L.G., Shwimer, J.S., Davis, S.J., and Rosen, D.I., "A Compact Vacuum Ultraviolet Light Source Based Upon Dielectric-Barrier Discharge Technology," PSI2229/TR-1261, final report to NASA/Goddard Space Flight Center under contract no. NASA CR-NASS-32437 (1993).

22. Piper, L.G., Cowles, L.M., Rawlins, W.T., "State-to-State Excitation of $NO(A\,^2\Sigma^+$ v'=0,1,2) by $N_2(A\,^3\Sigma_u+$, v'=0,1,2)," J. Chem. Phys. 85, 3369 (1986).

23. Piper, L.G., "Energy transfer studies on $N_2(X^1\Sigma_g^+, v)$ and $N_2(B^3\Pi_g)$," J. Chem. Phys. 97, 270 (1992).

24. Piper, L.G., "State-to-State $N_2(A\,^3\Sigma_u^+,)$ Energy-Pooling Reactions. 1. The Formation of $N_2(C^3\Pi_u)$ and the Herman Infrared System," J. Chem. Phys. 88, 231 (1988).

25. Knowles, P.G., Werner, H-J, Hay, P.J. and Cartwright, D.C., "The $A\,^2\Pi$--$X\,^2\Sigma^+$ red and $B\,^2\Sigma^+$--$X\,^2\Sigma^+$, violet systems of the CN radical: Accurate multireference configuration interaction calculations of the radiative transition probabilities," J. Chem. Phys. 89, 7334 (1988).

26. Levron, D. and Phelps, A.V., "Quenching of $N_2(A^3\Sigma_u^+, v=0, 1)$ by N_2, Ar, and H_2, "J Chem. Phys. 69, 2260 (1978).